biomass

MDPI

Article

Cascading Valorization of Residual Chestnut Biomass: Linking Aqueous Extraction, Reverse Osmosis, Spray Drying, and Solid Reuse

Pablo Fernández Santos [1], Claudia García-Revuelta [1], Lucía García-Flórez [1], Maria Amelia González-Arrojo [1], José Ramón Álvarez Saiz [2] and Susana Luque [2,*]

[1] Forest and Wood Technology Research Centre (CETEMAS), Pumarabule S/N, Carbayín Bajo, 33936 Siero, Principality of Asturias, Spain; marrojo@cetemas.es (M.A.G.-A.)
[2] Department of Chemical and Environmental Engineering, University of Oviedo, Julián Clavería 8, 33006 Oviedo, Principality of Asturias, Spain
* Correspondence: sluque@uniovi.es

Abstract

Residual chestnut biomass was evaluated in a cascading valorization route combining hot-water extraction, extractant reuse, reverse osmosis (RO), spray drying, and subsequent use of the extracted solid. Two heterogeneous residual *Castanea sativa* streams were studied at laboratory and pilot scale. Successive extraction at 100 °C recovered up to 141 mg gallic acid equivalents (GAE) g^{-1} dry biomass as Folin-reactive TPC, with 90–93% of the seven-stage response recovered after four fresh-water stages. Reusing the liquid on fresh biomass increased Folin-reactive TPC to 12.0–24.0 mg GAE mL^{-1}. Ultrafiltration did not provide useful fractionation, whereas RO gave >99.9% apparent Folin-reactive TPC retention and 96.5–97.6% total-solids retention; standard batches achieved 86.7–93.5% volume reduction. Carrier-free laboratory spray drying gave a maximum dry-solids collection recovery of approximately 60–62% in the favorable region near 20% feed solids. A representative powder contained 488 ± 27 mg GAE g^{-1} dry matter, showed a DPPH IC_{50} of 13.7 ± 1.1 µg mL^{-1}, water activity of 0.5850, and a volume-median particle size d_{50} of 7.42 µm. SEM showed predominantly spherical/sub-spherical particles together with hollow, concave, and partially collapsed particles. Complementary FTIR, MALDI-TOF, SEC-GPC, and qualitative on-flow ESI-MS provided structural and molecular-size fingerprints consistent with chestnut hydrolysable-tannin-related species, while individual assignments remain tentative. After two extraction cycles, residual biomass retained a net calorific value of 18.1–18.2 MJ kg^{-1} dry basis, although pellet durability decreased. The results define practical trade-offs linking liquid-product recovery and solid-residue valorization in an integrated chestnut-biomass cascade.

Keywords: chestnut biomass; cascading valorization; hot-water extraction; phenolic-rich extract; extractant reuse; reverse osmosis; spray drying; residual biomass

Check for updates

Academic Editor: Paolo Defilippis

Received: 22 August 2026
Revised: 23 September 2026
Accepted: 28 September 2026
Published: 9 October 2026

Copyright: © 2026 by the authors. Licensee MDPI, Basel, Switzerland. This article is an open access article distributed under the terms and conditions of the Creative Commons Attribution (CC BY) license.

1. Introduction

The transition toward a circular bioeconomy requires lignocellulosic residues to be considered not only for direct energy conversion or bulk solid uses, but also as sources of extractable chemical fractions that can be recovered before subsequent material or energy conversion. Cascading valorization follows this principle by sequentially obtaining

products of different value from the same biomass resource while preserving the remaining solid for further use [1,2]. Such an approach is particularly attractive for woody biomass because extractives represent only a fraction of the dry matter, whereas most of the cellulose–hemicellulose–lignin matrix remains after aqueous extraction and can potentially enter a second valorization route.

European chestnut (*Castanea sativa* Mill.) generates heterogeneous residual biomass from forestry operations and chestnut-related activities. Chestnut wood is particularly rich in hydrolysable tannins and other phenolic compounds, and chestnut extracts have long been used commercially in applications such as leather tanning and adhesives, while their antioxidant, antimicrobial and other functional properties have stimulated interest in additional bio-based applications [3,4]. The chemical profile of chestnut extractives depends on anatomical fraction, geographical origin and extraction conditions. Chromatographic studies have identified ellagitannins, gallic- and ellagic-acid derivatives and other phenolic compounds in chestnut wood and related tissues [5,6]. Accordingly, analytical responses obtained using the Folin–Ciocalteu assay should be interpreted as total phenolic/reducing capacity rather than as a direct quantification of individual tannins [7].

Water is an attractive extraction medium for the recovery of these compounds because it avoids organic solvents and facilitates subsequent aqueous processing. The extraction of tannins and phenolic compounds from chestnut biomass has, however, already been extensively investigated. Gironi and Piemonte studied the influence of temperature and solvent composition on polyphenol extraction from chestnut wood, while Capparucci et al. described both extraction kinetics and solid–liquid equilibrium in aqueous systems [8,9]. More recently, Aimone et al. demonstrated the scale-up of tannin extraction from chestnut wood waste from laboratory to semi-industrial conditions, and other studies have shown that phenolic composition and extractability depend strongly on the chestnut fraction and extraction sequence [6,10,11]. These contributions establish the feasibility of aqueous recovery and provide useful kinetic and compositional information, but they primarily address extraction as an individual operation.

For process implementation, the extraction stage cannot be considered independently from the concentration of the resulting liquid stream. Extensive washing of a biomass batch with fresh water can maximize recovery from the solid but simultaneously generates increasingly dilute extracts and increases the downstream water-removal requirement. An alternative is to reuse an already enriched liquid phase with fresh biomass, progressively increasing solute concentration while reducing the amount of water introduced into the process. This distinction is especially relevant for heterogeneous forestry residues, for which biomass origin, particle-size distribution and extraction history can strongly affect mass transfer. Thus, successive solid exhaustion and extractant reuse represent two different process strategies: the former prioritizes maximum recovery from a given biomass batch, whereas the latter prioritizes concentration of the liquid product and efficient use of the extraction medium [12,13].

Downstream concentration is therefore a key interface in an integrated process. Pressure-driven membrane operations are particularly attractive for aqueous plant extracts because water can be removed without the latent-heat requirement associated with evaporation. Ultrafiltration and nanofiltration have been used to fractionate or concentrate phenolic-rich streams from different agro-industrial residues, whereas reverse osmosis can provide high overall retention when selective fractionation is neither feasible nor required [14,15]. Membrane-assisted valorization has also been investigated for chestnut-processing by-products, demonstrating that pressure-driven separations can recover valuable phenolic compounds from chestnut-derived aqueous streams [15]. However, the most appropriate membrane is determined by the actual process objective: when pheno-

lics, carbohydrates and other dissolved compounds exhibit similar retention, attempted fractionation may increase process complexity without producing sufficiently differentiated fractions, whereas global preconcentration may be more useful for a subsequent stabilization step.

Conversion of the concentrated extract into a stable dry product introduces another process constraint. Spray drying offers short residence times and continuous conversion of liquid extracts into powders, but its performance strongly depends on feed-solids concentration, viscosity, feed temperature, atomization conditions and wall deposition [16,17]. Increasing feed concentration reduces the amount of water that must be evaporated, but excessive concentration can impair pumping and atomization and thereby reduce solids recovery. Consequently, membrane concentration and spray drying define a coupled operating window: the membrane step should remove sufficient water to reduce the thermal burden of drying, but not necessarily concentrate the extract to the maximum attainable value if the resulting feed becomes difficult to atomize.

A cascading approach also requires consideration of the solid remaining after extraction. Removal of the water-soluble fraction does not necessarily imply that the lignocellulosic residue loses its value as a fuel or material feedstock. Recent studies on detannized chestnut wood have demonstrated that the post-extraction solid can remain suitable for additional valorization routes [2]. Therefore, evaluating only phenolic recovery would provide an incomplete assessment of the biomass resource; the properties of the extracted solid must also be considered when determining whether the extraction step genuinely creates an additional product rather than simply transferring value from one fraction to another.

Against this background, the present work evaluates a cascading route for two real heterogeneous residual *C. sativa* biomass streams, linking aqueous extraction and extractant reuse with membrane preconcentration, spray drying, product benchmarking, and subsequent use of the extracted solid. Previous chestnut studies have demonstrated efficient aqueous or subcritical-water extraction and, in some cases, membrane fractionation or subsequent spray drying [6,10,15]. However, to the best of our knowledge, none has experimentally evaluated this complete sequence while also following the downstream energy and pelletization behavior of the extracted lignocellulosic solid, nor applied the same process framework to two distinct residual chestnut biomass streams. Laboratory and pilot-scale campaigns were therefore used to identify the trade-offs between solute recovery, liquid concentration, dryer operability, and residual-solid quality.

2. Materials and Methods

2.1. Experimental Program

Table 1 summarizes the process stages and sub-studies, their scale, experimental scope, and objective.

Table 1. Overview of the experimental program. The table is intentionally limited to scale and experimental scope; detailed objectives and procedures are described in the corresponding subsections.

Process Block	Scale	Experimental Scope
Biomass characterization	Raw material	LR and LC: particle-size distribution, moisture, bulk density, ash, GCV and NCV
Extraction screening	Pilot	70, 85 and 100 °C; S/L 1:10 and 1:13; up to 120 min
Particle size and kinetics	Laboratory	LR and LC as chipped, 4 mm and 1 mm fractions; 0–8 h; duplicate runs
Successive exhaustion	Laboratory	LR, LC and LR-4 mm; seven successive 8-h cycles with fresh water; duplicate runs
Extractant reuse	Laboratory	LR, LC and LR-4 mm; eight successive 8-h contacts of the same liquid with fresh biomass; duplicate runs
Pilot reuse validation	Pilot	Fresh-water extraction and reuse of first-cycle extract with a fresh biomass charge
Membrane screening	Laboratory	Ten membranes in dead-end filtration; five representative membranes in cross-flow
RO pressure study	Pilot	Stepped pressure sequence from 5 to 30 bar under total recirculation
RO batch concentration	Pilot	Multiple 10-bar batches; measured final VRF 7.5–15.3
RO concentration limit	Pilot	Pooled retentates from six independently concentrated batches

Table 1. *Cont.*

Process Block	Scale	Experimental Scope
RO permeability/cleaning	Pilot	Two consecutive concentration batches, water rinsing and detergent cleaning
Spray-drying window	Laboratory	Feed preheating; 1–3 bar atomization; 1–30 wt.% solids; 110–180 °C inlet air
Dry-product characterization	Laboratory	This-work powder and commercial references; TPC/DPPH/ash, a_w, laser diffraction, SEM, FTIR, MALDI-TOF, SEC-GPC and on-flow ESI-MS
Residual solid	Pilot-derived solid	Before extraction and after one/two extraction cycles; pelletization comparison

2.2. Raw Materials and Reagents

Two heterogeneous residual biomass streams from European chestnut (*Castanea sativa* Mill.) were used throughout the study. The chipped materials were supplied by Grupo Siero S.A. (Los Cuetos, Siero, Asturias, Spain). The first material, designated LR, consisted of chipped biomass originating from forestry operations and sawmilling residues. The second material, designated LC, consisted of chipped residual biomass obtained from old chestnut trees locally known as *cabornos*. Both materials were conditioned before characterization and extraction.

The original chipped materials were used directly in the pilot-scale extraction experiments and in part of the laboratory study. Additional particle-size fractions were produced using a Retsch SM 100 cutting mill (Retsch GmbH, Haan-Gruiten, Germany) fitted with 4 and 1 mm outlet screens. These milled materials were considered particle-size fractions derived from LR or LC and not independent feedstocks.

Type-II deionized water was used as the extraction solvent and ultrapure water for analytical procedures. Gallic acid, Folin–Ciocalteu reagent, sodium carbonate, methanol, 2,2-diphenyl-1-picrylhydrazyl (DPPH), and the remaining analytical reagents were of analytical grade. Ultrasil 125 alkaline detergent was used for membrane cleaning.

2.3. Biomass Characterization

The initial biomass was characterized in terms of particle-size distribution, moisture content, bulk density, ash content, gross calorific value (GCV), and net calorific value (NCV). These properties were selected to describe both feedstock heterogeneity during extraction and the suitability of the remaining solid for subsequent energy valorization.

Particle-size distribution was determined by oscillating sieving following the principles of UNE-EN ISO 17827-1 and UNE-EN ISO 17827-2. Sieves with nominal apertures of 45, 31.5, 16, 8, 3.15, and 1 mm were used. For each biomass, two subsamples of 1.0 ± 0.2 kg were sieved for 15 min in a Retsch AS 400 oscillating sieve shaker at 100 rpm, reversing the oscillation direction every 5 min. A third subsample was analyzed when the repeatability criterion was not fulfilled.

Moisture was determined following UNE-EN ISO 18134-2 by oven drying at 105 °C to constant mass. Two independent subsamples of 400 ± 100 g were analyzed; constant mass was considered to have been reached when the difference between two consecutive weighings separated by 1 h was below 0.2% of the initial sample mass. Biomass moisture was additionally determined before each extraction experiment so that biomass charges and extraction yields could be expressed on a dry-mass basis.

Ash content was determined in duplicate following UNE-EN ISO 18122 by calcination at 550 °C. Bulk density was measured following UNE-EN ISO 17828 using normalized containers selected according to biomass particle size; three independent determinations were performed for each biomass and values were expressed on wet and dry bases.

GCV and NCV were determined according to UNE-EN ISO 18125 using a Parr 6400 isoperibolic calorimeter (Parr Instrument Company, Moline, IL, USA). Biomass was ground and the fraction passing a 0.5 mm sieve was used. Calorimetric determinations were performed in duplicate and reported on a dry basis.

2.4. Analytical Characterization of Liquid and Dry Extracts

TPC was determined using the Folin–Ciocalteu method adapted to a 96-well microplate format from Singleton and Rossi [18]. Gallic acid was used as standard and a new seven-point calibration curve was prepared for each analytical series. Before analysis, a 1 mL aliquot of liquid extract was filtered through a 0.45 µm PVDF syringe filter and diluted with ultrapure water when required. In each well, 10 µL of blank, standard, or diluted sample were mixed with 215 µL ultrapure water, 15 µL Folin–Ciocalteu reagent, and 60 µL sodium carbonate solution (200 mg mL^{-1}). The reaction was maintained for 30 min at 37 °C and absorbance was measured at 750 nm using a Synergy HT microplate reader (BioTek Instruments, Winooski, VT, USA). Each analytical sample was measured in triplicate.

Results for liquid extracts were expressed as mg gallic acid equivalents (GAE) mL^{-1} and, when referred to the initial biomass, as mg GAE g^{-1} dry biomass. Because the Folin–Ciocalteu assay responds to reducing species beyond individual phenolic compounds, including some carbohydrates and degradation products, TPC is used here as an operational Folin-reactive response expressed as GAE and is not interpreted as a compound-specific phenolic or tannin concentration [7]. Extraction yields are therefore described as Folin-reactive TPC where this distinction is relevant, and membrane results as apparent Folin-reactive TPC retention.

TSC was determined gravimetrically using two independent aliquots per sample. Aliquots of 1 mL were used for laboratory extracts and 2 mL for pilot extracts. Samples were first dried at 70 °C until the visible liquid phase had disappeared and then at 103 °C for 24 h. Results were expressed as g L^{-1} or, when related to the initial biomass, as mg g^{-1} dry biomass.

Antioxidant capacity was determined for selected liquid and dry extracts using the DPPH radical-scavenging assay. Samples were analyzed in triplicate after 30 min reaction at 25 °C and absorbance was measured at 517 nm. Antioxidant capacity was expressed as IC_{50} (µg mL^{-1}), with lower values indicating higher radical-scavenging activity.

For dry products, 50 mg of powder was dissolved and made up to 100 mL with ultrapure water before TPC and DPPH analysis. Appropriate dilutions were prepared as required. Recovered dry products were stored in closed containers until characterization.

Total carbohydrate content (TCH) was determined when required for membrane-selection experiments using the anthrone colorimetric method, with D(+)-glucose as standard. Absorbance was measured at 620 nm and results were expressed as glucose equivalents.

Physical and Complementary Characterization of Dry Extracts

Water activity (a_w) of the process-derived powder and the SILVATEAM and PROTENSIL reference extracts was measured using a LabMaster-aw neo instrument equipped with an electrolytic sensor (Novasina AG, Lachen, Switzerland), following the measurement principle described in ISO 18787:2017 [19]. Measurements were taken on the solid products after equilibration in the measurement chamber.

Particle-size distribution of the process-derived powder was determined by laser diffraction using a Malvern Mastersizer 2000 equipped with a Scirocco 2000 dry-dispersion accessory (Malvern Panalytical, Malvern, United Kingdom). Results were expressed on a volume basis as d_{10}, d_{50}, d_{90}, surface-weighted mean diameter $D[3,2]$, volume-weighted mean diameter $D[4,3]$, span, and specific surface area. Particle morphology was examined by scanning electron microscopy (SEM) using a Quanta instrument at multiple magnifications.

Complementary structural characterization of the process-derived powder and commercial chestnut extracts was performed during a short research stay at LERMaB (Uni-

versity of Lorraine, France). ATR-FTIR spectra were compared by band position and fingerprint pattern. MALDI-TOF spectra were acquired in linear mode using a Shimadzu Biotech Axima Performance instrument and used as a qualitative mass-range fingerprint. Size-exclusion chromatography (SEC-GPC) of acetylated extract provided a calibrated apparent molecular-weight distribution based on calibration markers. Both the differential distribution curve and the cumulative distribution were evaluated; SEC values are reported as hydrodynamic-size descriptors rather than as compound identities. On-flow ESI-MS analysis was used as a complementary qualitative fingerprint.

2.5. Aqueous Extraction

2.5.1. General Laboratory Procedure

Laboratory extractions were carried out using Type-II water at a dry-biomass-to-water ratio of 1:10 (1 g dry biomass per 10 mL water). Each experiment used 35 g dry biomass and 350 mL water in a 500 mL round-bottom flask fitted with a reflux condenser. Extraction was performed at 100 °C without external mechanical stirring; liquid circulation was generated by boiling. Aliquots of 5 mL were withdrawn at the predefined sampling times and were not replaced. Duplicate extraction runs were performed for every experimental condition.

2.5.2. Particle-Size and Kinetic Experiments

The effect of particle size on extraction kinetics was evaluated for both LR and LC using three physical forms: original chipped biomass, the fraction obtained using a 4 mm mill screen, and the fraction obtained using a 1 mm mill screen. Extraction was monitored for 8 h, with samples collected at 0, 0.25, 0.5, 1, 2, 3, 4, 6, and 8 h. The time-zero sample was taken immediately after mixing biomass and water followed by approximately 10 s of manual agitation. TPC and TSC profiles were used to compare extraction rate and the approach to a concentration plateau. The 8-h duration was a kinetic/exhaustion characterization window and is not proposed as an industrial residence time; the later pilot reference condition was 100 °C, S/L = 1:10, and 120 min.

2.5.3. Successive Biomass Exhaustion

Successive extraction experiments were performed to determine the progressively extractable fraction when the same biomass was repeatedly contacted with fresh water. Chipped LR, chipped LC, and the 4 mm fraction of LR were each subjected to seven consecutive 8-h extraction cycles under the general conditions described above. Two independent experimental replicates were performed for each material.

At the end of each cycle, the liquid extract was separated through a 40 µm stainless-steel mesh. The extracted biomass was allowed to cool and drain overnight and was then contacted with fresh water for the next cycle. The nominal process ratio was 1:10; in these exhaustion runs, 360 mL were charged at the start of each cycle to provide a sampling allowance for the sequential 5-mL aliquots, which reduced the in-flask liquid volume to approximately 340 mL by the 8-h sample. Mean liquid recovered after separation was approximately 280 mL for chipped LR and LC and 250 mL for LR-4 mm. Samples were collected at 0, 1, 2, 4, and 8 h during each cycle. Cumulative extraction yield was calculated from the concentrations and recovered liquid volumes of all extracts generated up to each stage and was expressed relative to the initial dry biomass.

2.5.4. Extractant Reuse

A complementary multistage experiment was designed to investigate enrichment of the liquid phase rather than exhaustion of a single biomass batch. Chipped LR, chipped LC, and the 4 mm fraction of LR were evaluated. Each experiment started with 350 mL water and one fresh biomass charge. After each 8-h extraction cycle, the biomass was separated

through a 40 µm stainless-steel mesh and discarded. The recovered extract was retained for the following cycle and its volume was restored to 350 mL with fresh water to compensate for liquid retained by the biomass and sampling losses.

Approximately 280 mL of liquid was typically recovered after each cycle for chipped LR and LC, whereas approximately 250 mL was recovered for the 4 mm LR fraction. The reconstituted extract was then contacted with a new, previously unextracted biomass charge. Eight consecutive cycles were carried out, with two independent replicates for each material. Samples were collected at 0, 1, 2, 4, and 8 h in each cycle and analyzed for TPC and TSC.

2.5.5. Pilot-Scale Extraction and Process Validation

Pilot extraction experiments were carried out in a 220 L autoclave using the original chipped biomass. An initial screening campaign evaluated extraction temperatures of 70, 85, and 100 °C, dry-biomass-to-water ratios of 1:10 and 1:13, and extraction times up to 120 min after the target temperature had been reached.

The condition selected for subsequent pilot experiments was 100 °C, a 1:10 dry-biomass-to-water ratio, and 120 min extraction time. This condition was used to evaluate two process strategies: (i) successive extraction of the same biomass batch with fresh water and (ii) reuse of the extract obtained from a first biomass batch as extraction medium for a second fresh biomass charge. Liquid samples were characterized by TPC and TSC and, where relevant, by pH and conductivity. The pilot experiments tested whether the trends identified at laboratory scale remained observable with heterogeneous chipped biomass under a larger-scale hydrodynamic regime.

2.6. Kinetic and Equilibrium Modeling

The experimental TPC extraction profiles were fitted using a second-order extraction model and Peleg's empirical model. Goodness of fit was evaluated using the coefficient of determination (R^2) and mean absolute percentage deviation (MAPD):

$$\mathrm{MAPD}(\%) = \frac{100}{N}\sum_{i=1}^{N}\left|\frac{y_i^{\mathrm{exp}} - y_i^{\mathrm{pred}}}{y_i^{\mathrm{exp}}}\right|, \tag{1}$$

where N is the number of experimental points and y_i^{exp} and y_i^{pred} are the experimental and predicted values, respectively.

The second-order extraction model was written as

$$\frac{dC_t}{dt} = k(C_\infty - C_t)^2, \tag{2}$$

where C_t is the TPC yield at time t, C_∞ is the asymptotic TPC yield predicted by the model, and k is the second-order extraction constant. Integration gives

$$\frac{t}{C_t} = \frac{1}{kC_\infty^2} + \frac{t}{C_\infty}. \tag{3}$$

Peleg's model was written as

$$C_t = C_0 + \frac{t}{K_1 + K_2 t}, \tag{4}$$

where C_0 is the experimentally measured initial TPC yield, K_1 is the Peleg rate constant, and K_2 is the Peleg capacity constant. The initial extraction rate is $1/K_1$, while the asymptotic value predicted by the equation is

$$C_\infty = C_0 + \frac{1}{K_2}. \tag{5}$$

Equilibrium states obtained from the biomass-exhaustion and extractant-reuse experiments were represented by relating the TPC remaining in the solid, q_e (mg GAE g^{-1} dry biomass), to the equilibrium TPC concentration in the liquid, C_e (mg GAE mL^{-1}). Langmuir and Freundlich expressions were fitted to the pooled equilibrium dataset at 100 °C:

$$q_e = \frac{Q_{max} K_L C_e}{1 + K_L C_e}, \tag{6}$$

$$q_e = K_F C_e^{1/n}. \tag{7}$$

Here, Q_{max} is the maximum solid-phase TPC predicted by the Langmuir model (mg GAE g^{-1} dry biomass), K_L is the Langmuir constant on the adopted liquid-concentration basis, K_F is the Freundlich constant on the corresponding mixed concentration basis, and $1/n$ is the Freundlich exponent. The models were used as empirical engineering descriptions of the experimental domain; no extrapolation beyond the studied feedstocks, temperature, and aqueous-extraction conditions was assumed.

Nonlinear and linear regressions were performed in MATLAB R2021b (MathWorks, Natick, MA, USA).

2.7. Membrane Processing

2.7.1. Membrane Screening and Selection

Membrane selection was performed in two stages. The preliminary screening comprised ten flat-sheet membranes spanning nanofiltration, ultrafiltration, and reverse osmosis, with different polymeric materials and nominal separations. Their identifiers and nominal characteristics are summarized in Table 2. The preliminary tests were performed in Amicon 8050 dead-end cells (Merck KGaA, Darmstadt, Germany) with a working volume of 50 mL and an effective membrane area of 0.00134 m^2. Two independently cut membrane coupons were evaluated for each membrane; a third was tested when appreciable differences in hydraulic response were observed. Pure-water permeability was first determined, followed by extract filtration at 4 bar until sufficient permeate had been collected for analytical characterization. Permeate flux and apparent retention of TSC and TPC were used as the primary screening criteria.

Five membranes representing different productivity-retention compromises were then evaluated under cross-flow conditions in a GE Osmonics SEPA CF II module with an effective membrane area of 0.0145 m^2. Extract filtration was performed at 4 bar and a retentate flow of 100 L h^{-1} after a 90-min total-recirculation stabilization period. TSC, TPC, TCH, and DPPH response were measured in the relevant feed, retentate, and permeate samples. Hydraulic permeability was determined before extract processing, after a water rinse, and after subsequent alkaline-detergent cleaning when required. In these cross-flow selection experiments, the cleaning sequence consisted of 30 min with water at 20 °C, followed by 30 min with 0.5% Ultrasil 125 detergent solution and a final 40-min water rinse. This procedure was used to distinguish material removable by water rinsing from the residual loss of permeability that required chemical cleaning.

Table 2. Membranes included in the screening program. Commercial separation and maximum-pressure information refers to manufacturer or supplier specifications; experimental configuration and area refer to this study.

Code	Manufacturer/Model	Type	Material	Nominal Separation	Max. P (bar)	Experimental Mode
NA-PESH30k	Microdyn-Nadir UH030	UF	hydrophilic PES	30 kDa	10	dead-end
AL-PS25k	Alfa Laval GR60PP	UF	PS/PP	25 kDa	10	dead-end
AL-RC10k	Alfa Laval RC70PP	UF	regenerated cellulose/PP	10 kDa	10	dead-end + cross-flow
SY-PES10k	Synder ST	UF	PES	10 kDa	8	dead-end + cross-flow
SY-PES5k	Synder MT	UF	PES	5 kDa	8	dead-end + cross-flow
NA-PESH4k	Microdyn-Nadir UH004	UF	hydrophilic PES	4 kDa	10	dead-end + cross-flow
SU-PA3k	SUEZ/Veolia GK	UF/NF	PA-TFC	~3 kDa PEG class	27.6	dead-end
SY-PES3k	Synder VT	UF	PES	3 kDa	8	dead-end
SU-PA1k	SUEZ/Veolia GE	NF	PA-TFC	~1 kDa PEG class	27.6	dead-end
DD-RO	DuPont FilmTec SW30-2540	RO	PA-TFC	99.7% stabilized NaCl rejection	83	spiral-wound pilot

Active membrane area was 0.00134 m^2 for dead-end tests, 0.0145 m^2 for cross-flow tests, and 2.8 m^2 for the spiral-wound RO element.

2.7.2. Pilot Reverse-Osmosis Unit and Pressure Study

Pilot concentration was carried out using a spiral-wound FilmTec™ SW30-2540 thin-film composite polyamide RO module (DuPont) with an active membrane area of 2.8 m^2. Before entering the RO unit, the chestnut extract was passed sequentially through 50 and 5 µm prefilters. The system comprised a 120 L feed tank, pressure regulation, retentate-flow control, and temperature control. Retentate flow was maintained at 1000 L h^{-1} and feed temperature at 20 ± 1 °C.

Before each pressure step, permeate and retentate were returned to the feed tank so that the extract concentration remained approximately constant. The pressure sequence was 5, 10, 5, 15, 10, 20, 15, 25, 20, 30, and 25 bar. At every pressure level, permeate flux was monitored until no further variation in flux was observed before the next pressure change was applied. The alternating ascending and descending sequence allowed the hydraulic response at a given pressure to be compared before and after exposure to a higher pressure. Retentate and permeate samples were collected at the established pressure levels for TPC and TSC determination.

The apparent retention of component i was calculated as

$$R_i = \left(1 - \frac{C_{p,i}}{C_{r,i}}\right) \times 100, \quad (8)$$

where $C_{p,i}$ and $C_{r,i}$ are the concentrations of component i in permeate and retentate, respectively.

2.7.3. Batch Concentration and Practical Concentration Limit

Batch concentration experiments were performed at 10 bar, 1000 L h^{-1} retentate flow, and 20 ± 1 °C. Individual experiments started from approximately 120 L of prefiltered extract. Retentate was continuously recycled to the feed tank while permeate was removed from the system. Permeate flow was measured repeatedly and each operating point was considered stabilized when no further variation in flux was observed.

Retentate and permeate samples were collected during concentration for TSC and TPC analysis. Individual batches were concentrated down to the minimum practical operating volume of the pilot plant, corresponding to a volume reduction of approximately 90% and VRF values of approximately 10 under the standard batch procedure.

A separate high-concentration experiment was conducted to explore the practical limit of operation. Six independently concentrated retentates were pooled and the combined enriched feed was concentrated again at 10 bar. Paired retentate and permeate samples

of approximately 25 mL were collected at 13 points during this high-concentration run. TPC, TSC, and permeate flux were monitored until the flux became too low for stable further concentration.

2.7.4. Pilot RO Hydraulic-Permeability Recovery and Cleaning

Changes in pilot RO hydraulic permeability during repeated use were evaluated using two consecutive batch-concentration experiments without alkaline-detergent cleaning between batches. Pure-water hydraulic permeability was measured initially at 2, 5, and 10 bar. After the first extract batch had been concentrated, the unit was emptied and subjected to a water rinse; hydraulic permeability was then measured again. A second extract batch was subsequently concentrated under the same operating conditions, followed by a second water rinse and a third permeability measurement.

This sequence distinguished the permeability loss remaining after water rinsing from the recovery subsequently obtained by cleaning with a detergent solution. Routine post-experiment cleaning consisted of a 30-min water rinse, followed by recirculation of a 1% (m/v) Ultrasil 125 alkaline-detergent solution for 45 min and a final 30-min water rinse.

2.8. Spray Drying

Laboratory spray-drying experiments were performed in a LabPlant SD5 unit (LabPlant, North Yorkshire, UK) equipped with a variable-speed peristaltic feed pump and a two-fluid atomization nozzle. The feed was continuously mixed during each experiment. Approximately 400 ± 50 mL of feed was processed per run. Unless otherwise stated, the feed rate was maintained at 5 ± 0.5 g min^{-1} and the drying-air flow at 56 m^3 h^{-1}.

The experimental program was performed sequentially. First, the effect of feed preheating was evaluated at feed temperatures of 25 and 60 °C using feeds containing 10 and 20 wt.% TSC. Based on this study, 60 °C was selected as the feed temperature for subsequent experiments.

Second, atomization pressure was evaluated at 1, 2, and 3 bar using a 10 wt.% TSC feed preheated to 60 °C. A pressure of 1 bar was selected for the final experimental series.

Finally, the combined effects of feed-solids concentration and inlet-air temperature were evaluated using feeds containing 1, 5, 10, 20, and 30 wt.% TSC and inlet-air temperatures of 110, 145, and 180 °C. All 15 concentration-temperature combinations were tested at a feed temperature of 60 ± 5 °C and an atomization pressure of 1 bar.

Before and after each experiment, the product collector, drying chamber, and cyclone were weighed. Dry-solids collection recovery, R_{coll}, was calculated as the dry mass of powder recovered in the final product collector divided by the dry-solids mass introduced with the feed, multiplied by 100; collected powder mass was corrected for its measured moisture. Chamber and cyclone deposition, outlet-air temperature, and final powder moisture were recorded as additional indicators of dryer performance and operability. Material retained in non-weighed parts of the atomization system and fine particles leaving the single cyclone with the exhaust were not independently recovered and therefore contribute to the unaccounted fraction. The reported recovery is consequently a collection recovery for this laboratory configuration rather than a true chemical product yield.

A separate product-quality comparison was performed using powder obtained from the RO-concentrated residual-biomass extract at three drying-air temperature conditions spanning approximately 110–180 °C. TPC, DPPH antioxidant response, and residual powder moisture were measured for these dried products. These experiments were used to determine whether the process conditions that improved physical recovery also produced a systematic deterioration in the global phenolic or antioxidant response. Recovered solid products were stored in closed containers until characterization.

2.9. Benchmarking and Qualitative Mass-Spectral Characterization of the Dry Extract

A representative dry extract obtained through the process route developed in this work (hot-water extraction, RO concentration, and spray drying) was benchmarked against two commercial chestnut extracts, SILVATEAM and PROTENSIL. The three powders were analyzed for TPC, ash content, and DPPH antioxidant response. TPC was expressed as mg GAE g^{-1} dry matter and DPPH response as IC_{50} (μg mL^{-1}). Ash content was defined and determined gravimetrically as the residue remaining after calcination of a previously dried sample, following UNE-EN ISO 18122. The dried material was placed in conditioned porcelain crucibles and calcined in an LVT/9/11/P330 muffle furnace (Nabertherm GmbH, Lilienthal, Germany). The temperature program comprised heating to 250 °C over 30 min, holding at 250 °C for 60 min, heating to 550 °C over 30 min, and holding at 550 °C for 120 min. After cooling to room temperature in a desiccator, the residue was weighed and expressed relative to the dry sample mass.

Qualitative mass-spectral fingerprints were obtained using a Shimadzu LC-20A system (Shimadzu, Kyoto, Japan) coupled to a Shimadzu LC-MS 8030 triple-quadrupole mass spectrometer equipped with an electrospray-ionization interface. The analysis was performed on-flow without a chromatographic column, using HPLC-grade water containing 0.1% formic acid as the carrier solution. For each extract, 1 mL of a 2 mg mL^{-1} solution in ultrapure water was mixed with 0.1 mL DMSO to improve solubilization, and 2 μL were injected.

Nitrogen was used as drying and nebulizing gas at 15 and 3 L min^{-1}, respectively. The heat-block and desolvation-line temperatures were 400 and 250 °C. The ion-spray voltage magnitude was 4500 V. Spectra were acquired by electrospray ionization in negative mode over m/z 100–3000. Because no chromatographic separation, authentic standards, or targeted MS/MS confirmation was used in this preliminary comparison, compound assignments were considered tentative and based on diagnostic m/z values reported for chestnut hydrolysable tannins [5,6].

2.10. Characterization and Downstream Use of the Extracted Biomass

The energetic properties of LC were determined before extraction and after the first and second pilot extraction cycles. GCV and NCV were measured according to the same standardized calorimetric procedure used for the initial biomass, allowing direct comparison of the specific energy content before and after removal of the water-soluble fraction.

Pelletization experiments were carried out with non-extracted and extracted chestnut biomass using the industrial pelletization procedure available at the collaborating facility. The resulting pellets were characterized in terms of mechanical durability and fines content according to the applicable solid-biofuel procedures. These tests were not intended to optimize pellet production but to determine whether hydrothermal extraction introduced a measurable penalty in the subsequent energy-oriented use of the residual lignocellulosic solid.

2.11. Replication and Data Treatment

Extraction experiments were performed in duplicate unless otherwise stated, and analytical TPC measurements were performed in triplicate. Biomass characterization used the replicate structure specified in Section 2.3. The preliminary membrane screen used two independently cut coupons per membrane, with a third coupon when the hydraulic response differed appreciably. The pilot RO pressure sequence, high-concentration RO experiment, spray-drying screening conditions, and pelletization comparison were engineering runs rather than replicated factorial experiments. Error bars and "±" values are

shown only where replicate or repeated analytical measurements were available; single-run screening values are reported without implied statistical uncertainty.

Stagewise material quantities were expressed on the reference bases stated in Table 10. Extraction was normalized to 1000 kg initial dry LR biomass. RO was summarized by the measured feed and final concentrations; the dry-solids content of the final concentrate was calculated as $m_{TS} = VC_{TSC}$ on a 1000 L concentrate basis, with consistent units. Spray-drying collection was calculated for 1000 kg liquid feed at 20 wt.% TSC using the measured dry-solids collection recovery. These stage-specific calculations use results from the separate experimental campaigns.

3. Results and Discussion

3.1. Process Concept and Characteristics of the Residual Feedstocks

Figure 1 summarizes the cascading process evaluated in this work: aqueous extraction and liquid reuse, membrane preconcentration, spray drying, and subsequent valorization of the extracted solid. Downstream water removal and residual-solid quality were therefore treated as process constraints rather than as independent end points.

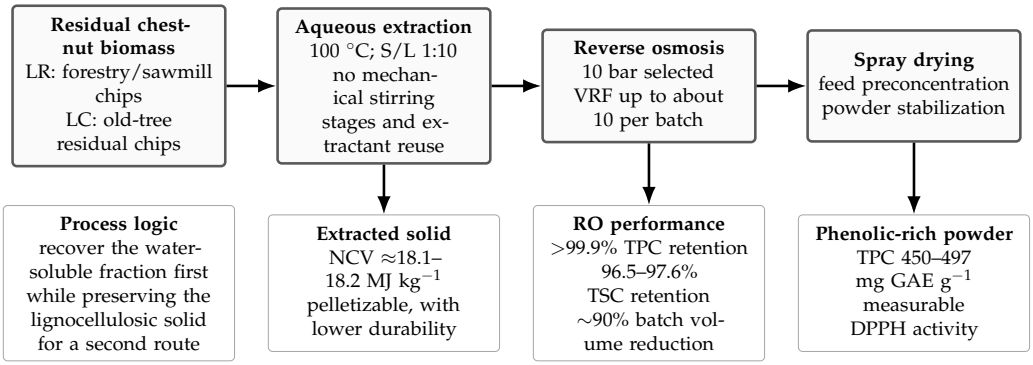


Figure 1. Cascading valorization concept evaluated in this work. Extraction and membrane concentration were developed from laboratory to pilot scale, whereas spray drying of the residual-biomass-derived extract was evaluated at laboratory scale. The scheme represents the experimentally supported process route rather than a continuously coupled pilot line.

The two residual-biomass streams had similar moisture, low ash contents, and closely comparable gravimetric calorific values (Table 3). Their principal difference was physical rather than energetic.

Table 3. Main characteristics of the two residual chestnut-biomass feedstocks.

Parameter	LR	LC
Moisture after conditioning (%)	12.97	13.22
Bulk density, wet basis (kg m^{-3})	233.3 ± 1.2	259.3 ± 1.2
Bulk density, dry basis (kg m^{-3})	203.1	225.1
Ash, dry basis (%)	0.450 ± 0.052	0.323 ± 0.021
Gross calorific value, dry basis (MJ kg^{-1})	19.46	19.17
Net calorific value, dry basis (MJ kg^{-1})	18.12	17.82
Net volumetric energy density (GJ m^{-3} dry basis)	3.68	4.01

Direct structural composition (cellulose, hemicellulose, lignin, and total extractives) was not determined. Published data provide context for the expected range in *C. sativa* wood: Jusic et al. reported 7.12% extractives, 36.66% cellulose, 13.90% hemicellulose, and 31.89% lignin in virgin chestnut wood chips, compared with 4.02, 37.78, 13.40, and 29.38%, respectively, after industrial detannization [2]. The differences observed here may therefore reflect anatomical composition, extractive content, particle structure, and processing history.

The LC stream also contained a visibly greater bark contribution than the conventional LR stream. This feature is relevant because bark is particularly rich in water-soluble extractives in *C. sativa*. Kakavas et al. reported hot-water-soluble extractives of 26.33% in bark, compared with 19.22% in heartwood and 7.08% in sapwood [20]. Chestnut bark extracts also contain hydrolysable tannins and related phenolic compounds, including vescalin, castalin, vescalagin, castalagin, gallic acid, and ellagic acid [21]. The greater bark contribution in LC may therefore contribute to its higher Folin-reactive extraction response, although the bark fraction was not quantified separately.

LC had an approximately 11% higher dry-basis bulk density than LR and consequently a higher net volumetric energy density (4.01 versus 3.68 GJ m^{-3}), despite its slightly lower NCV on a mass basis (Table 3). This higher bulk density is consistent with the finer particle-size distribution of LC, which may promote more efficient packing of the chipped biomass.

Particle-size distribution further differentiated the two materials (Figure 2). LR was dominated by the 16–31.5 mm fraction, which represented 44.21% of the total mass. LC showed a markedly finer distribution, with 35.27% in the 8–16 mm fraction and 18.11% below 3.15 mm. Overall, 78.35% of LC was below 16 mm compared with 54.43% of LR. The two feedstocks therefore differed not only in extraction response but also in particle-size distribution and handling characteristics, providing a clear physical basis for their distinct behavior during solid–liquid processing.

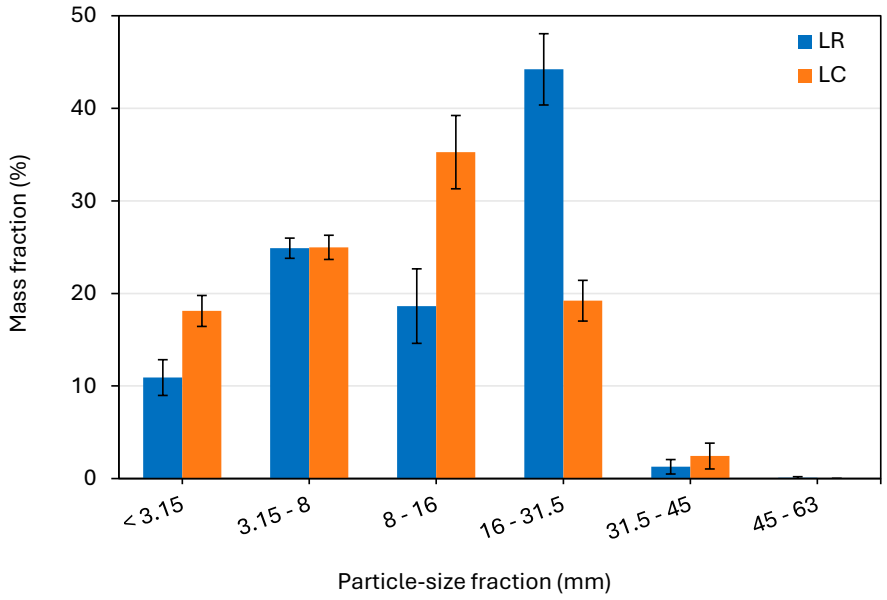


Figure 2. Particle-size distributions of LR and LC residual chestnut biomass. Values correspond to the combined mass fractions obtained from duplicate sieving determinations.

3.2. Designing the Aqueous Extraction Stage

3.2.1. Pilot Screening and Selection of Reference Operating Conditions

The pilot screening covered biomass origin, temperature, solid-to-liquid ratio, and extraction time. Across the campaign, TSC ranged from approximately 2.52 to 10.62 mg mL^{-1} and TPC from 1.00 to 4.87 mg GAE mL^{-1}, confirming a strong dependence on feedstock and operating conditions.

The key conditions used to select the reference point are summarized in Table 4. At the selected 100 °C, S/L = 1:10, 120-min condition, LC produced a higher TPC yield than LR (46.52 versus 34.04 mg GAE g^{-1} dry biomass) and a more concentrated extract (Table 4).

Table 4. Selected pilot extraction results illustrating the effects of feedstock and solid-to-liquid ratio at 100 °C and 120 min.

Biomass	S/L	TSC (mg mL^{-1})	Gravimetric Yield (% Dry Biomass)	TPC (mg GAE mL^{-1})	TPC Yield (mg GAE g^{-1})
LR	1:10	7.30	6.96	3.57	34.04
LR	1:13	5.13	6.74	2.26	29.72
LC	1:10	10.62	10.14	4.87	46.52

For LR, increasing water availability from S/L = 1:10 to 1:13 decreased both TPC and TSC concentrations without increasing gravimetric or TPC yield (Table 4). The additional water therefore generated a more dilute stream and motivated the later emphasis on liquid reuse and membrane preconcentration. This trend is also consistent with Khatib et al., who found that increasing the water-to-solid ratio did not necessarily increase tannin recovery from chestnut wood, whereas temperature exerted a stronger effect [6].

LC gave the higher response, but tree age, anatomical position, and origin were not independently controlled; the difference is therefore treated as a feedstock effect associated with real residual-biomass heterogeneity rather than assigned mechanistically to age [6]. On this basis, 100 °C, S/L = 1:10, and 120 min were selected as a reference condition for pilot process development. This was a process-development choice, not a formal statistical optimum.

3.2.2. Particle Size, Kinetics, and Practical Milling Limit

Reducing particle size markedly accelerated phenolic extraction, but further milling below 4 mm did not provide a consistent increase in final recoverable TPC. Chipped LR continued to increase throughout the 8-h experiment and therefore did not reach a well-defined plateau within the observation window. The corresponding LC chips also continued to increase, although the rate diminished at long extraction times. In contrast, the milled materials approached their high-TPC region substantially earlier. This behavior shows that milling primarily reduces the characteristic extraction time rather than necessarily increasing the equilibrium extractable fraction.

The second-order model described the kinetic datasets more consistently than Peleg's equation. Across the tested LR and LC physical forms, second-order fits gave $R^2 \geq 0.9869$ and MAPD $\leq 4.2\%$, whereas Peleg fits reached lower R^2 values, down to 0.8788, and MAPD values up to 8.4%. The fitted Peleg parameters were particularly sensitive to the non-zero concentration measured at the first sampling point for the finer material. The practical implication is that moderate milling can remove an important mass-transfer limitation, whereas more severe size reduction adds preprocessing without a measurable gain in final TPC recovery.

3.2.3. Successive Extraction: Operational Biomass Exhaustion

The seven-cycle exhaustion experiment quantified both the total recoverable fraction and the diminishing contribution of successive fresh-water stages (Figure 3). Final cumulative TSC recoveries were 187 ± 5, 283 ± 5, and 229 ± 6 mg g^{-1} dry biomass for LR, LC, and LR-4 mm, respectively. Corresponding cumulative TPC values were 81 ± 8, 141 ± 7, and 125 ± 8 mg GAE g^{-1}.

The first extraction stage accounted for approximately 51, 54, and 60% of the seven-stage TPC for LR, LC, and LR-4 mm, respectively. After three stages, 83–87% of the final seven-stage TPC had been recovered, and after four stages this increased to approximately 90–93%. TSC showed the same front-loaded behavior: the first stage accounted for approx-

imately 55, 54, and 66% of the final seven-stage TSC, and more than 80% was recovered after three stages.

The final three stages were useful to approach an operational exhaustion criterion but contributed little additional recovery. Four stages are therefore a process-relevant reference point rather than a demonstrated economic optimum: beyond this point, the incremental recovery was small while each fresh-water contact generated another dilute stream. At the nominal S/L ratio of 1:10, extending the sequence from four to seven stages increases fresh-water demand from approximately 40 to 70 L kg^{-1} dry biomass (75% more water) for only the remaining 7–10% of the seven-stage Folin-reactive response.

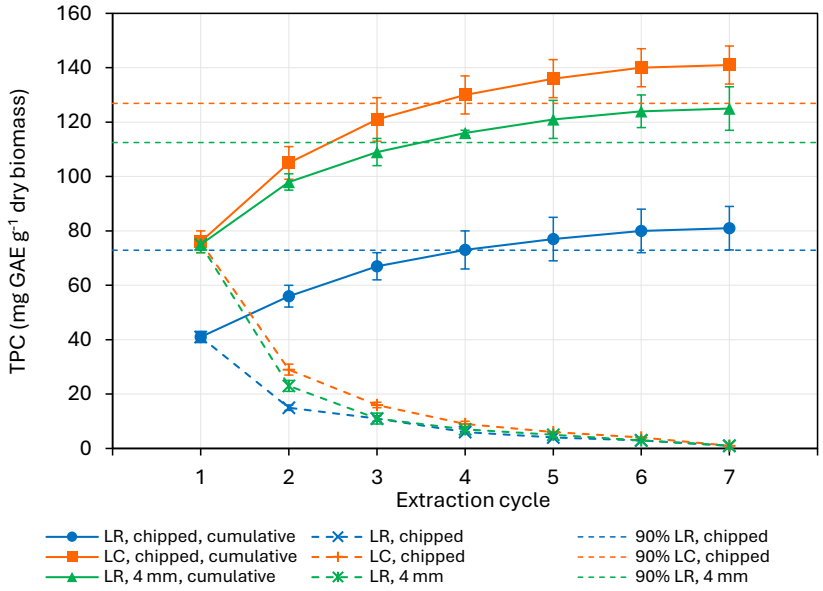


Figure 3. Folin-reactive TPC recovered during seven successive fresh-water extraction cycles on the same biomass batch. Solid lines show cumulative recovery, dashed lines the contribution of each cycle, and horizontal reference lines 90% of the final cumulative response for each material.

Pilot-scale sequential extraction confirmed the same diminishing-return behavior with chipped LR. The first pilot extraction recovered approximately 60.1 g GAE kg^{-1} dry biomass, whereas a second fresh-water extraction of the same solid contributed a further 22.0 g GAE kg^{-1}. The cumulative two-stage value therefore reached approximately 82.0 g GAE kg^{-1}, with the second stage contributing only about 27% of the two-stage total.

3.2.4. Extractant Reuse: Enriching the Liquid Phase

The complementary reuse experiment addressed the opposite process objective: increasing liquid-phase concentration while repeatedly using the same water inventory on fresh biomass (Figure 4). After eight cycles, TSC concentrations reached 24.8 ± 1.2, 40.6 ± 0.4, and 32.9 ± 1.3 mg mL^{-1} for LR, LC, and LR-4 mm, respectively. Corresponding TPC concentrations were 12.0 ± 0.0, 24.0 ± 0.5, and 18.3 ± 1.0 mg GAE mL^{-1}.

Enrichment was again strongly front-loaded. After four cycles, LR and LR-4 mm had reached approximately 83 and 89% of their final eight-cycle TPC concentration, respectively; LC had reached approximately 71%, reflecting its higher extractable content and continued enrichment in later contacts. This distinction is central to process design. Repeated fresh-water extraction maximizes recovery from one solid batch but creates several dilute streams, whereas liquid reuse sacrifices complete exhaustion of each biomass charge in favor of progressively increasing the solute load presented to the downstream membrane step.

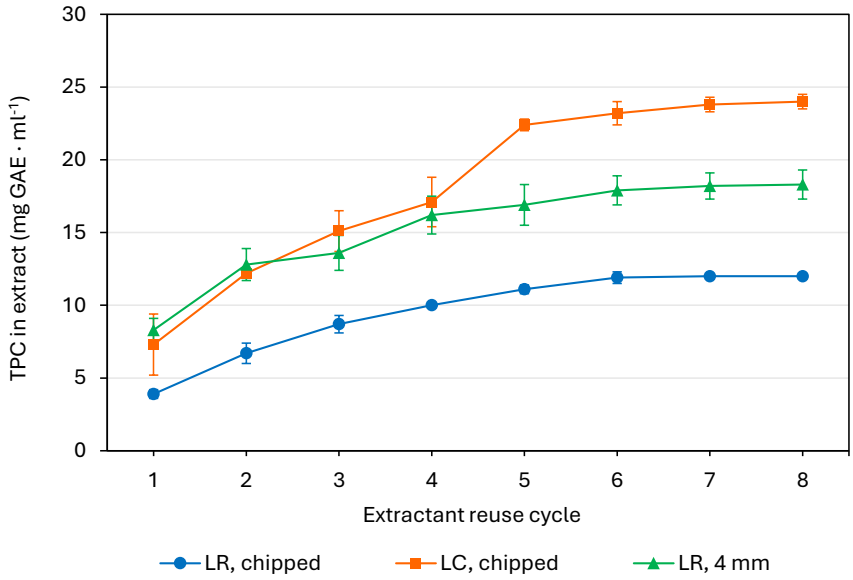


Figure 4. Increase in extract total phenolic content when the same liquid phase was reused on fresh biomass.

Repeated liquid reuse did not produce a systematic deterioration in DPPH response on a dry-extract basis. Between the first and eighth contacts, IC_{50} changed from approximately 14.7 to 10.4 μg mL^{-1} for LR, 11.1 to 8.8 for LC, and 12.6 to 8.7 for LR-4 mm. Because intermediate values were not monotonic, these data are used only to show that reuse did not measurably compromise the global radical-scavenging response.

Pilot validation further supported the reuse concept. After restoring the recovered first-cycle extract to the working volume, its TPC concentration at the start of the second pilot contact was approximately 2.16 g GAE L^{-1} and increased to 6.29 g GAE L^{-1} after contact with fresh biomass. TSC simultaneously increased from approximately 3.93 to 11.91 g L^{-1}. Conductivity increased from approximately 340 to 728 μS cm^{-1} and pH decreased from about 3.8 to 3.4, providing simple bulk indicators of solute accumulation. These pilot data do not establish an unlimited number of reuses, but they demonstrate that an already enriched aqueous phase retained substantial extraction capacity at larger scale.

3.2.5. Equilibrium Representation as a Process Descriptor

Combining the exhaustion and reuse states allowed the solid–liquid distribution of TPC at 100 °C to be represented with Langmuir and Freundlich expressions. Both models described the pooled dataset well, with $R^2 = 0.9775$ for Langmuir and $R^2 = 0.9770$ for Freundlich. The fitted Langmuir parameters were $K_L = 0.02832$ on the adopted liquid-concentration basis and $Q_{max} = 345$ mg GAE g^{-1} dry biomass, while the Freundlich parameters were $K_F = 13.01$ on the corresponding mixed concentration basis and $1/n = 0.75$.

The similarity of the two fits indicates that the experimental range does not justify assigning unique mechanistic significance to either model. Their value here is primarily descriptive: the common relationship captures the progressive decrease in extraction driving force as the liquid becomes enriched or the solid becomes depleted. The fact that LR, LC, and LR-4 mm could be represented within a common empirical relationship suggests that their principal differences are associated with the amount and accessibility of extractable material rather than fundamentally different equilibrium behavior.

Specific aqueous-extraction kinetics and equilibria for chestnut wood were previously reported by Capparucci et al. [9]; therefore, the contribution of the present model analysis is not the use of Langmuir or Freundlich equations itself. Its role is to connect the equilibrium

states generated by biomass exhaustion and liquid reuse to a multistage process-design framework. Applicability beyond comparable chestnut residues extracted with water at 100 °C should be independently validated.

3.3. Membrane Processing: From Attempted Fractionation to Global Preconcentration

3.3.1. Preliminary Screening: Productivity-Retention Trade-Off

The preliminary dead-end screening of ten membranes established the first important design decision for the downstream process. Permeate fluxes spanned more than one order of magnitude, from 2.9 L m^{-2} h^{-1} for SU-PA1k to 46.0 L m^{-2} h^{-1} for AL-RC10k, while apparent TPC retention ranged from 55.8 to 99.7%. The corresponding TSC retentions ranged from 56.3 to 97.5%. Figure 5 summarizes this productivity-retention trade-off.

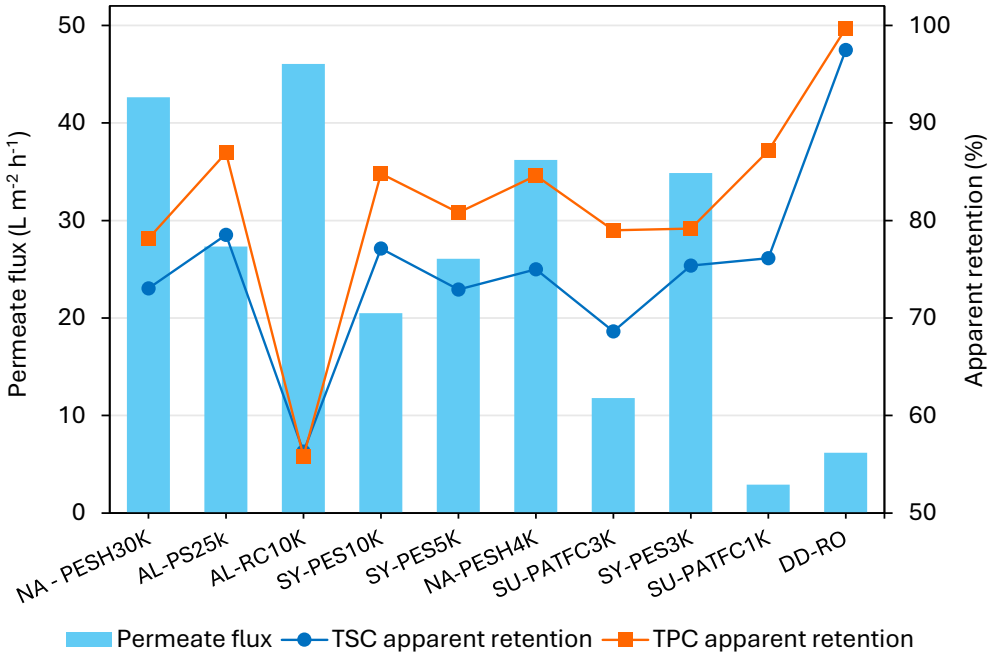


Figure 5. Dead-end membrane screening: permeate flux and apparent retention of TSC and TPC. Membranes are ordered by decreasing nominal pore-size/MWCO class, with RO shown last. Feed concentrations were 7.12 g L^{-1} TSC and 3.25 g GAE L^{-1} TPC.

AL-RC10k occupied the high-productivity/low-retention extreme, with 46.0 L m^{-2} h^{-1} and apparent retentions of 56.3% TSC and 55.8% TPC. DD-RO showed the opposite behavior: its flux was only 6.2 L m^{-2} h^{-1}, but TSC and TPC retentions reached 97.5 and 99.7%, respectively. The remaining membranes filled the intermediate region. For example, NA-PESH4k provided 36.2 L m^{-2} h^{-1} with retentions of 75.0% TSC and 84.6% TPC, whereas SY-PES5k and SY-PES10k provided intermediate fluxes and TPC retentions of approximately 80–85%.

For each membrane, TSC and TPC broadly followed the same retention trend. TSC and TPC retentions differed by at most 11 percentage points. Thus, nominal MWCO did not translate into a sufficiently strong differentiation between the global phenolic response and the remaining dissolved solids. This does not imply identical retention of individual molecular species; rather, the measured fractions were not differentiated strongly enough to justify a fractionation strategy on this basis.

3.3.2. Cross-Flow Confirmation and Membrane Cleanability

The second selection stage tested five representative membranes under cross-flow and added TCH as a third compositional response. The results reinforced the conclusion of the preliminary screening (Figure 6). AL-RC10k again gave the highest flux, 98.0 L m^{-2} h^{-1}, but retained only 68.2% of TSC, 70.5% of TPC, and 71.0% of TCH. NA-PESH4k offered the strongest ultrafiltration compromise, with a flux of 58.5 L m^{-2} h^{-1} and retentions close to 90% for all three analytical fractions. The two PES membranes gave lower fluxes, approximately 26 L m^{-2} h^{-1}, with intermediate retentions. DD-RO again provided the highest retention, with values of 97.5% for TSC, 99.8% for TPC, and 99.7% for TCH.

The similarity of TSC, TPC, and TCH retention within each membrane is particularly important. A membrane such as NA-PESH4k could retain roughly 90% of the measured soluble fractions at a substantially higher flux than RO, but it did not preferentially enrich TPC relative to carbohydrates or total dissolved matter. Conversely, the lower-MWCO PES membranes did not provide a clear selectivity advantage despite their lower fluxes. This behavior is consistent with work on complex plant extracts showing that nominal MWCO alone is insufficient to predict phenolic/carbohydrate fractionation because solute size distributions, association between solutes, and solute–membrane interactions all contribute to the observed separation [22–24].

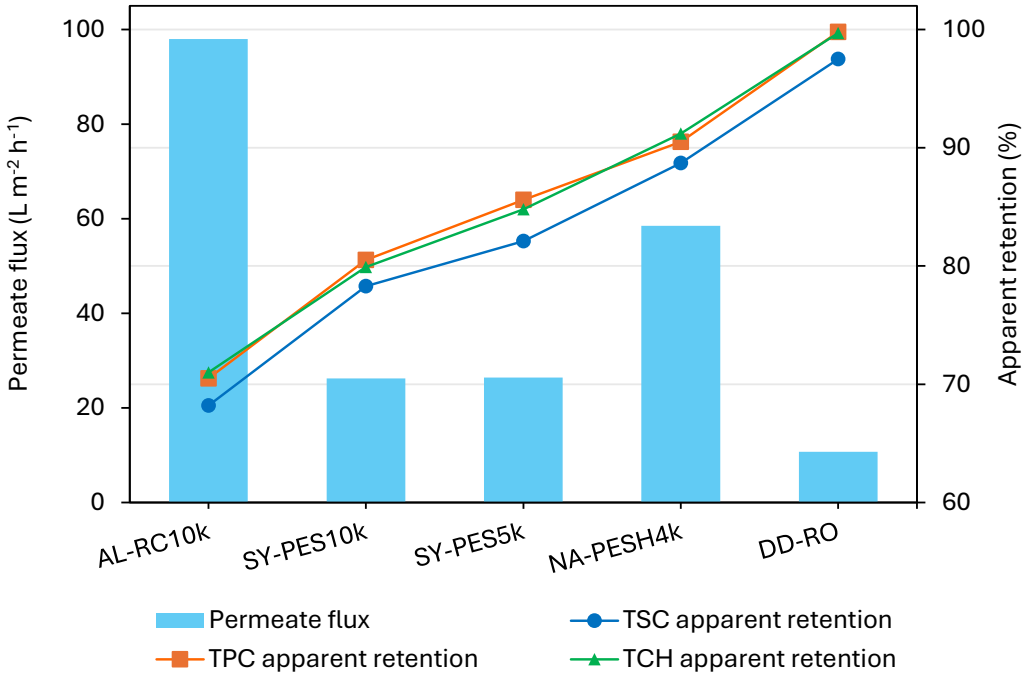


Figure 6. Cross-flow permeate flux and apparent retention of total solids (TSC), total phenolic content (TPC), and total carbohydrates (TCH) for the five membranes retained after preliminary screening. Membranes are ordered by decreasing nominal pore-size/MWCO class, with RO shown last.

Hydraulic-permeability recovery added a second selection criterion (Figure 7). AL-RC10k and NA-PESH4k recovered approximately 90 and 92% of their initial permeability after water rinsing alone. The PES membranes recovered only about 70–74% after water rinsing, but subsequent alkaline cleaning increased recovery to approximately 94–98%. DD-RO behaved similarly: water rinsing recovered about 72% of the initial permeability, whereas alkaline cleaning restored approximately 98%. NA-PESH4k reached an apparent recovery of about 118% after chemical cleaning. A value above 100% indicates that the post-cleaning hydraulic state differed from the initial state and should not, by itself, be interpreted as proof of membrane degradation or improved intrinsic permeability.

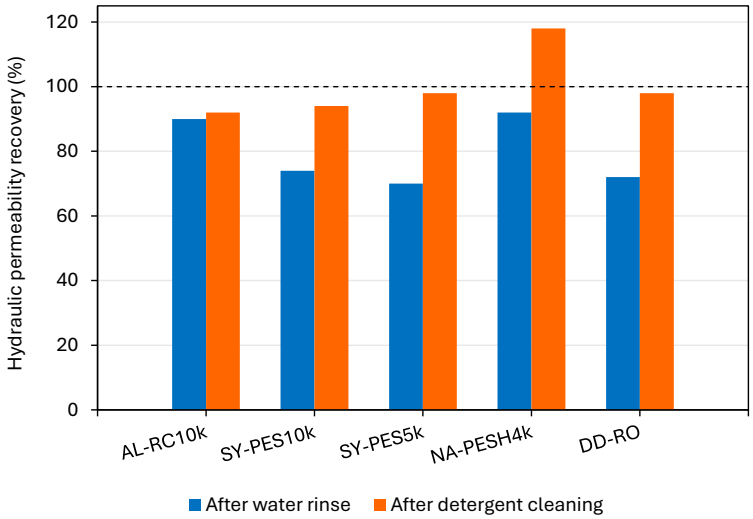


Figure 7. Recovery of pure-water hydraulic permeability after water rinsing and after subsequent alkaline-detergent cleaning for the membranes evaluated in the second selection stage. Membranes are displayed in the same decreasing nominal pore-size/MWCO order as in Figure 6, with RO shown last. Values are expressed relative to the initial hydraulic permeability.

The cleaning results therefore did not identify a single membrane that was superior in every criterion. AL-RC10k was easy to recover hydraulically but transmitted roughly 30% of the global phenolic response. NA-PESH4k was the strongest UF candidate when productivity and retention were weighted together. DD-RO had the lowest flux, but virtually eliminated loss of TPC and TCH to the permeate. Because the downstream objective was concentration before drying rather than production of selectively fractionated streams, the process criterion shifted from maximum flux to maximum recovery of the soluble product.

The resulting RO performance is competitive with the upper range reported for phenolic-rich plant extracts. Tapia-Quirós et al. reported approximately 91–99% TPC rejection with NF membranes and more than 99.9% with RO for winery and olive-mill extracts [14]. Similarly, Alsobh et al. obtained >99% TPC retention with an X-20 RO membrane for anise and hawthorn extracts, whereas NF270 remained below 90% [25]. The >99.9% apparent TPC retention observed here therefore lies at the upper end of these reported values and supports RO as the appropriate option when global phenolic recovery, rather than fractionation, is the objective.

This behavior is consistent with other plant-extract studies, in which useful polyphenol/carbohydrate fractionation depends strongly on the membrane/feed system and may require diafiltration or adsorption in addition to UF [22,23,26]. For the present chestnut extract, forcing a fractionation objective would add complexity without generating sufficiently differentiated global fractions.

3.3.3. Pilot RO: Pressure Selection and Hydraulic Hysteresis

Once DD-RO had been selected, a stepped-pressure experiment was performed at approximately constant bulk concentration. The first increase from 5 to 10 bar raised the stabilized permeate flux from approximately 13 to 25 L m^{-2} h^{-1}. Returning to 5 bar restored essentially the original flux. Above this range, however, the hydraulic response became progressively history-dependent (Figure 8). The ascending branch reached approximately 29 L m^{-2} h^{-1} at 15 bar, 31 at 20 bar, and 33 at 25 bar; increasing pressure to 30 bar produced almost no further gain. When pressure was subsequently reduced to previously tested values, the stabilized flux was systematically lower than on the preceding upward step.

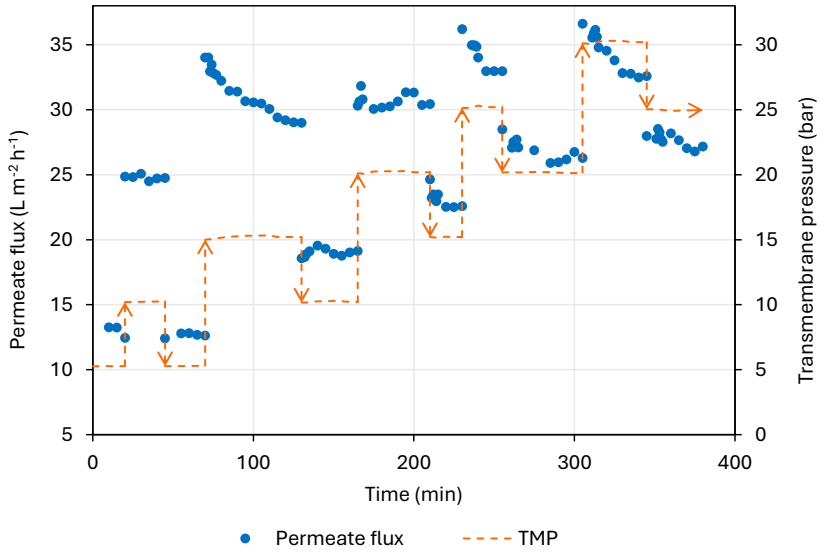


Figure 8. Permeate flux during the stepped-pressure experiment, together with the imposed transmembrane-pressure (TMP) sequence. The divergence observed after the first low-pressure recovery illustrates the progressive hydraulic hysteresis developed during the pressure-cycle test.

The pressure cycle therefore identified two simultaneous effects. First, the flux-pressure relationship became increasingly non-linear above approximately 15–20 bar, indicating diminishing hydraulic returns from additional pressure. Second, the lower return fluxes showed that exposure to the higher-pressure states altered the hydraulic resistance of the system over the timescale of the experiment. The available data cannot separate membrane compaction, concentration polarization, and deposited-material resistance quantitatively, so the observed hysteresis is interpreted as an overall change in hydraulic state rather than assigned to a single mechanism.

In contrast to flux, solute retention was largely insensitive to pressure. Across 5–30 bar, TPC retention remained above 99.9%, while TSC retention varied only from approximately 96.5 to 97.6%. The feed contained approximately 3.55 g GAE L^{-1} TPC and 6.96 g L^{-1} TSC. Thus, increasing pressure above 10 bar increased hydraulic demand and eventually produced only small flux gains without materially improving solute retention. A working pressure of 10 bar was therefore selected for the prolonged concentration experiments.

3.3.4. Batch Concentration and Practical Concentration Limit

At 10 bar, RO strongly reduced extract volume while maintaining the phenolic response in the retentate. Across four recorded pilot batches, volume reduction ranged from 86.7 to 93.5% (final VRF approximately 7.5–15.3), showing that major water removal was reproducible across separate engineering runs. As concentration proceeded, however, permeate flux fell continuously. In the high-concentration experiment, flux declined from 25.7 L m^{-2} h^{-1} at the beginning of the enriched-feed run to 1.4 L m^{-2} h^{-1} at VRF = 5 (Figure 9). Expressing the VRF axis logarithmically makes the near-logarithmic decline of permeate flux explicit.

The concentration increase accompanying this loss of productivity was substantial (Figure 10). TSC rose from approximately 79 to 284 g L^{-1} and TPC from approximately 35.7 to 164 g GAE L^{-1} over the final concentration run. At the endpoint, the corresponding permeate concentrations were only about 1.9 g L^{-1} TSC and 0.7 g GAE L^{-1} TPC. The retained-liquid concentration therefore increased strongly while solute transmission remained small relative to the retentate concentration.

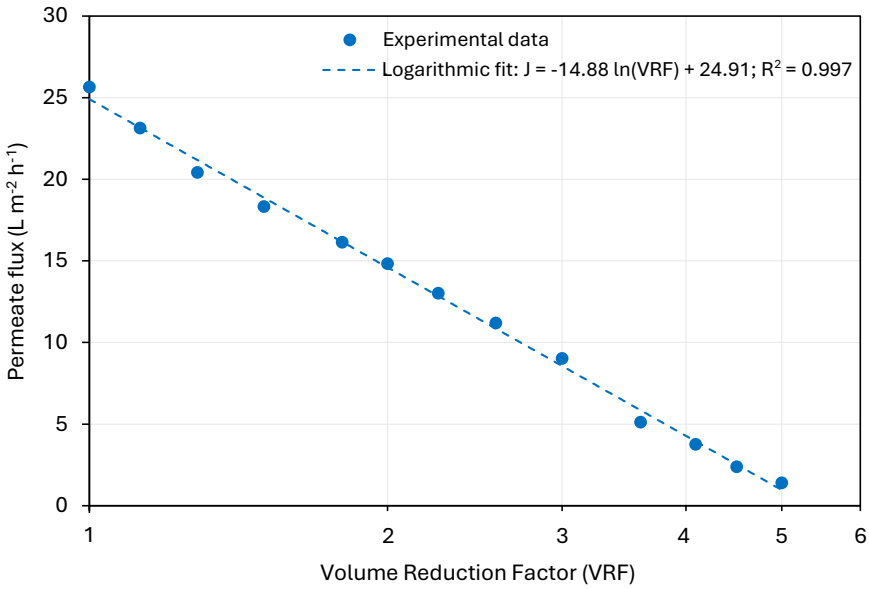


Figure 9. Permeate-flux decline during the final high-concentration RO experiment as a function of volume reduction factor. The x-axis is shown on a logarithmic scale and the line corresponds to the logarithmic fit.

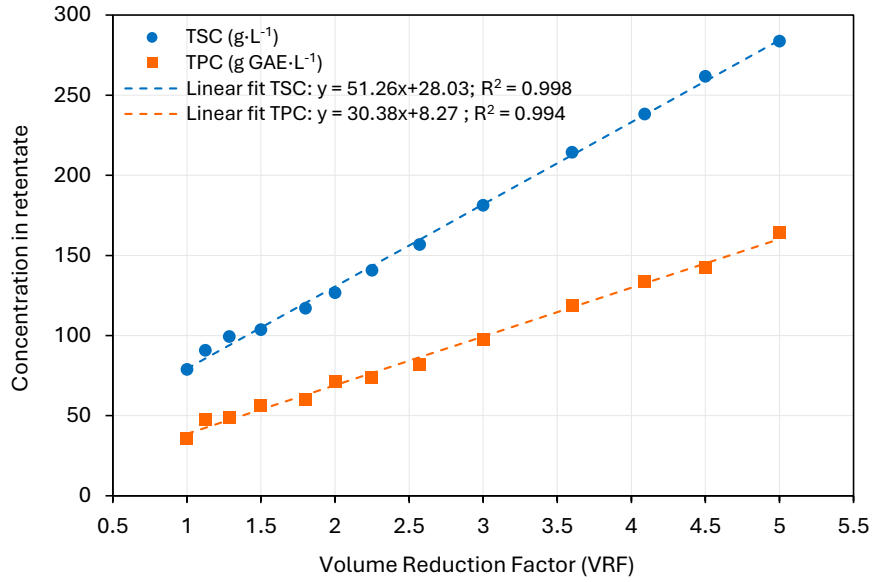


Figure 10. Retentate total-solids concentration (TSC) and Folin–Ciocalteu total phenolic content (TPC) during the final high-concentration RO experiment, together with linear-fit lines.

A semilogarithmic mass-transfer representation of the terminal concentration region yielded apparent zero-flux concentrations of approximately 288 g L^{-1} for TSC and 166 g GAE L^{-1} for TPC, close to the measured maxima of 284 and 164 g L^{-1}, respectively. Both extrapolations were close to the measured maxima, supporting use of the relationship as an empirical descriptor of the limiting region under the studied hydrodynamic conditions. It does not demonstrate a unique thermodynamic solubility limit.

The observed flux decline is consistent with several effects that become increasingly important as a complex extract is concentrated: increasing osmotic pressure reduces the effective driving force for water transport; increasing viscosity raises hydraulic resistance; concentration polarization increases the solute concentration near the membrane surface;

and deposition or other fouling phenomena can add further resistance. The present experiments do not resolve these contributions independently. The relevant process conclusion is instead that the technically achievable concentration is not set only by membrane retention: productivity collapses as the concentrate approaches the high-solids region.

The concentration levels reached are also high relative to representative plant-extract studies. Conidi et al. obtained 30.16 g L^{-1} total polyphenols in the NF retentate of aqueous chestnut-shell extracts [15]. Lai et al. concentrated waste tea-leaf extract by RO to a concentration factor of 7.57, obtaining 25.82 g GAE L^{-1} polyphenols and 64.62 g L^{-1} total solids in the retentate, with recovery yields of 85.1 and 83.7%, respectively [27]. In the present limiting-concentration experiment, the measured values approached 164 g GAE L^{-1} TPC and 284 g L^{-1} TSC. These absolute concentrations are markedly higher, but direct performance ranking is not appropriate because feedstocks, pressures, membrane objectives, and analytical methods differ. Together with the approximately 90% volume reduction achieved in standard batches, the comparison nevertheless confirms that the concentration range obtained here is technically relevant for downstream powder production.

This result creates the key interface with spray drying. RO can remove a large fraction of the process water while retaining essentially all of the measured phenolic response, but operating to the maximum attainable RO concentration is not necessarily desirable if the resulting concentrate exceeds the pumping and atomization window of the dryer. The membrane stage should therefore be terminated at a concentration selected jointly with downstream drying requirements rather than at the highest concentration that can be reached hydraulically.

3.4. Spray Drying: Defining the Stabilization Window

The spray-drying study was organized as a sequence of operating decisions. Feed preheating to 60 °C improved dry-solids recovery, particularly at 20% TSC, and reduced residual powder moisture. At 10% TSC and 60 °C, increasing atomization pressure from 1 to 3 bar reduced recovery while increasing chamber deposition, with only a small moisture benefit (Table 5). Accordingly, 60 °C feed temperature and 1 bar atomization pressure were retained for the final concentration–temperature matrix.

Table 5. Laboratory spray-drying screening used to select feed temperature and atomization pressure. Recovery is reported on a dry-solids basis.

Condition	Product Recovery (%)	Chamber Deposit (g)	Product Moisture (%)
10% TSC, feed 25 °C	50.8	12.2	6.7
10% TSC, feed 60 °C	53.0	10.8	5.2
20% TSC, feed 25 °C	54.1	21.6	6.4
20% TSC, feed 60 °C	60.1	20.7	4.8
10% TSC, 1 bar	53.0	10.8	5.2
10% TSC, 2 bar	50.5	12.1	5.0
10% TSC, 3 bar	48.7	12.7	4.8

The complete drying dataset, including chamber deposition, powder moisture, and outlet-air temperature, is provided in Supplementary Table S1.

Once feed temperature and atomization pressure had been fixed, feed-solids concentration and inlet-air temperature were studied jointly over 1–30% TSC and 110–180 °C (Table 6). Feed-solids concentration exerted the stronger influence on recovery. At 180 °C, recovery increased from approximately 35% at 1% TSC to 50% at 5%, 56% at 10%, and 62% at 20% TSC. Increasing concentration further to 30% reduced recovery to approximately 50%. The same non-monotonic dependence on feed solids was observed at the lower inlet temperatures.

Table 6. Dry-basis product recovery (%) for the complete laboratory spray-drying matrix. Feed temperature was 60 °C and atomization pressure was 1 bar.

Feed TSC (%)	Inlet-Air Temperature		
	110 °C	**145 °C**	**180 °C**
1	31	33	35
5	42	47	50
10	54	55	56
20	58	60	62
30	46	47	50

The temperature effect was comparatively modest within the investigated range. At 20% TSC, increasing inlet temperature from 110 to 145 and 180 °C increased recovery only from approximately 58 to 60 and 62%, respectively. Thus, a 70 °C increase in inlet temperature improved dry-solids recovery by only about four percentage points. Even at 110 °C, no accumulation of undried liquid feed was observed in the lower collection vessel at the applied throughput, indicating that the evaporative capacity of the laboratory dryer was sufficient at this condition.

The decrease in recovery at 30% TSC is especially important for integration with RO. At this concentration, greater wall deposition and intermittent feed-line obstruction were observed. Therefore, reducing the water load by membrane concentration is beneficial only while the concentrate remains pumpable and atomizable. The maximum concentration attainable by RO and the maximum concentration that can be processed efficiently by the dryer are not the same design target. For the laboratory equipment, approximately 20% TSC represented the most favorable operating region observed between solids loading and spray-dryer operability; because the screening was not a replicated factorial study, this is not interpreted as a statistically established optimum.

The maximum dry-solids collection recovery obtained here (approximately 60–62%) is competitive with values reported for other botanical extracts when the collection configuration and use of carriers are considered. Langrish and Premarajah reported peak recoveries of 65–70% for a spray-dried antioxidant-rich *Hibiscus sabdariffa* extract [28]. Gavarić et al. obtained 58.36% recovery for a carrier-free *Marrubium vulgare* extract and 77.07% after addition of 10% maltodextrin [29]. The approximately 60–62% recovery achieved in the present work is therefore slightly above the reported carrier-free value and was obtained without maltodextrin or another drying aid, thereby avoiding dilution of the phenolic-rich product.

The measured collection recovery should also be interpreted in the context of the laboratory collection system. The LabPlant SD5 used here recovers powder through a single cyclone, so fine particles not captured by that cyclone are not included in the gravimetric product recovery. Laboratory-scale spray dryers commonly show lower yields because of wall deposition and limited cyclone capture of fine particles; reported laboratory yields typically span approximately 20–70% [30]. Larger spray-drying installations may incorporate additional fines-recovery devices, such as secondary cyclones and/or particulate filters. Consequently, the 60–62% value is a performance measure for the laboratory dryer and its collection train rather than an intrinsic upper limit of the chestnut extract drying process. Higher overall recovery could reasonably be expected from a scaled collection system with dedicated fine-particle recovery, although this was not experimentally demonstrated in the present work.

Additional characterization of powders produced from the RO-concentrated residual-biomass extract showed that higher drying temperature did not produce a monotonic improvement in product quality (Table 7). The dried products contained approximately 487, 497, and 450 mg GAE g^{-1} dry product at the low, intermediate, and high

drying-temperature conditions, respectively. Their DPPH IC_{50} values were 15.15, 13.90, and 15.77 μg mL^{-1}. Across the three drying conditions, TPC ranged from 449.8 to 496.9 mg GAE g^{-1} (arithmetic mean 478.0 mg GAE g^{-1}), while DPPH IC_{50} ranged from 13.90 to 15.77 μg mL^{-1} (arithmetic mean 14.94 μg mL^{-1}). These across-condition means are descriptive and are not reported as replicate-derived uncertainty. Residual powder moisture decreased from approximately 9.8 to 7.4% over the same temperature range.

Table 7. Quality indicators of powders obtained from the RO-concentrated residual-biomass extract at three laboratory drying-temperature conditions. The intermediate condition was recorded as approximately 140–145 °C in the experimental files.

Drying Condition	TPC (mg GAE g^{-1} Dry Product)	DPPH IC_{50} (μg mL^{-1})	Powder Moisture (%)
Low, 110 °C	487.4	15.15	9.8
Intermediate, ~140–145 °C	496.9	13.90	8.88
High, 180 °C	449.8	15.77	7.40

Because the quality characterization was not designed as a replicated factorial comparison of temperature, these differences should not be interpreted as statistically significant temperature effects. Nevertheless, the data show that the high-temperature condition did not provide a quality advantage: it produced the lowest residual moisture but also the lowest measured TPC among the three powders, while antioxidant response remained in a similar range. Together with the relatively small gain in solids recovery above 110 °C, this result argues against increasing drying temperature simply to maximize recovery.

The drying results therefore define a coupled operating window with RO. RO should concentrate the extract sufficiently to reduce the water burden on the dryer, but not to the terminal membrane concentration if the resulting feed approaches the poor-atomization region. Conversely, increasing dryer temperature provides only limited recovery gains and can increase thermal severity. In the present equipment, a feed near 20% TSC, preheated to 60 °C and atomized at 1 bar, provided the most defensible reference window; inlet temperature can then be selected within the lower-to-intermediate part of the tested range according to the required final moisture and product-quality specification.

3.5. Benchmarking and Qualitative Composition of the Phenolic-Rich Powder

The powder obtained in this work was compared with two commercial chestnut extracts as reference products for phenolic and antioxidant responses (Table 8). It showed the highest TPC of the three products, while its DPPH IC_{50} was of the same order as SILVATEAM and markedly lower than PROTENSIL.

Table 8. Comparison of the process-derived powder obtained in this work with two commercial chestnut extracts. Values are expressed on a dry-matter basis where applicable.

Parameter	This Work	SILVATEAM	PROTENSIL
TPC (mg GAE g^{-1} dry matter)	488 ± 27	404 ± 1	122 ± 1
Ash (mg g^{-1} dry matter)	29.9 ± 0.2	15.2 ± 0.3	31.1 ± 0.6
DPPH IC_{50} (μg mL^{-1})	13.7 ± 1.1	10.6 ± 0.5	76 ± 2
Water activity, a_w	0.5850	0.5722	0.5880
d_{50} (μm)	7.420	–	8.741
d_{90} (μm)	15.726	–	17.819

Its ash content was close to that of PROTENSIL and approximately twice that of SILVATEAM, showing that the higher TPC did not correspond to a lower inorganic fraction.

Water activity was similar for the three powders: 0.5850 for the process-derived powder, 0.5722 for SILVATEAM, and 0.5880 for PROTENSIL. All three values were below 0.60 and closely comparable, providing an additional physical descriptor of the low-water-availability dry products. Laser diffraction showed a fine particle-size distribution for the process-derived powder (Figure 11), with $d_{10} = 3.208$, $d_{50} = 7.420$, and $d_{90} = 15.726$ µm, $D[3,2] = 4.412$ µm, $D[4,3] = 8.608$ µm, a span of 1.687, and a specific surface area of 1.36 $m^2\ g^{-1}$. PROTENSIL showed somewhat larger characteristic diameters ($d_{50} = 8.741$ µm and $d_{90} = 17.819$ µm).

SEM revealed a heterogeneous powder composed predominantly of spherical or sub-spherical particles together with hollow, concave, and partially collapsed particles and agglomerates of finer material (Supplementary Figure S1). Such morphologies are consistent with rapid shell formation followed by shrinkage or partial collapse during droplet drying.

Complementary ATR-FTIR, MALDI-TOF, and SEC-GPC further broadened the product characterization. Individual FTIR spectra and the fingerprint-region overlay are provided in Supplementary Figures S3 and S4; the MALDI-TOF spectra are provided in Supplementary Figures S5–S7. The process-derived extract and SILVATEAM showed closely corresponding FTIR band positions in the carbonyl, aromatic, galloyl/C–O, and carbohydrate regions (approximately 1720, 1600, 1308/1170–1180, and 1030 cm^{-1}), whereas PROTENSIL showed a less resolved galloyl-region fingerprint. These comparisons are based primarily on band position and pattern rather than absolute transmittance amplitude. MALDI-TOF provided a complementary qualitative mass fingerprint for the process-derived extract. Because laser powers differed among compared samples, MALDI signal intensity and simple peak count were not used quantitatively, and structural assignments remain tentative.

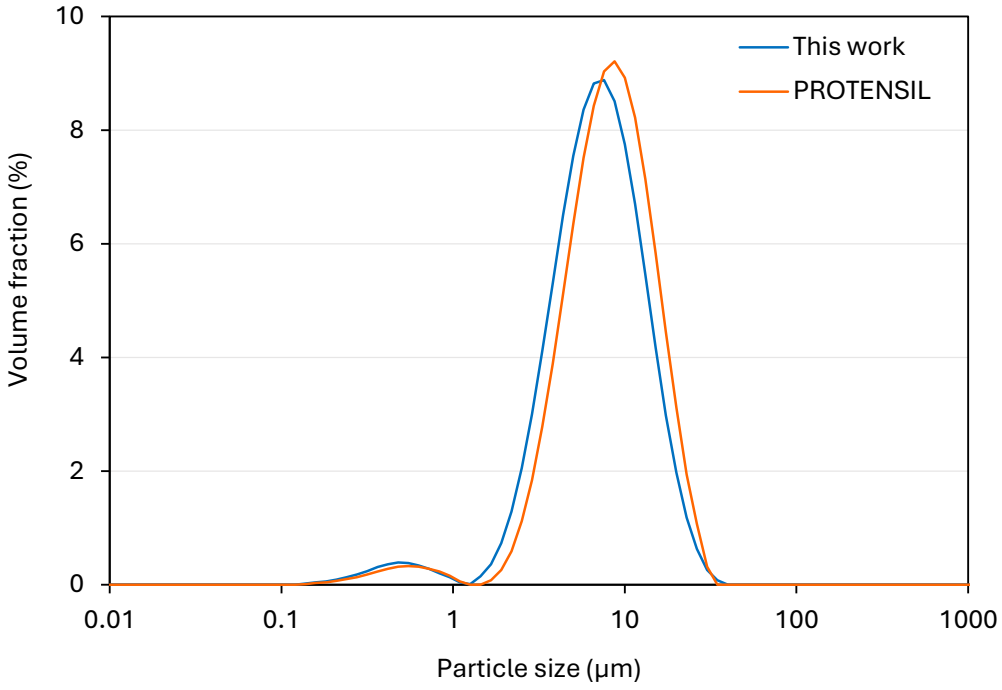


Figure 11. Laser-diffraction particle-size distribution of the spray-dried process-derived powder compared with PROTENSIL. Representative SEM micrographs of the powder are provided in Supplementary Figure S1.

SEC-GPC of the acetylated process-derived extract showed a broad calibrated apparent molecular-weight distribution (Supplementary Figure S2). The differential distribution

exhibited two principal apparent size regions centered around approximately 1 kDa and 5–6 kDa, together with a broader higher-molecular-weight tail. The cumulative distribution gave approximate descriptors of 0.53 kDa at the 10th percentile, 1.18 kDa at the 25th percentile, 3.97 kDa at the median, 11.2 kDa at the 75th percentile, and 32.9 kDa at the 90th percentile. These values describe calibrated hydrodynamic-size equivalents and are not interpreted as compound identities.

The qualitative negative-ion mass spectra provided an additional compositional check (Figure 12). The spectrum of the extract obtained in this work contained strong signals at approximately m/z 466 and 933, consistent with the doubly and singly deprotonated forms commonly assigned to the ellagitannin stereoisomer pair castalagin/vescalagin. A signal near m/z 631 was consistent with castalin/vescalin. Additional signals in the regions of m/z 331, 481, and 483 were consistent with monogalloyl-glucose, HHDP-glucose, and digalloyl-glucose, respectively [5,6]. The intense signal around m/z 313 may correspond to a galloyl-glucose-related fragment, but its assignment is treated cautiously because the analysis did not include chromatographic separation or targeted fragmentation confirmation.

The extract obtained in this work and SILVATEAM shared diagnostic regions near m/z 466, 631, and 933, supporting broadly similar spectral regions consistent with hydrolysable-tannin/ellagitannin-related species. PROTENSIL showed greater relative signal intensity in the lower-mass region and much weaker signals near m/z 631 and 933. Together with the TPC and DPPH results, this qualitative comparison supports classification of the product obtained in this work as a phenolic-rich chestnut extract.

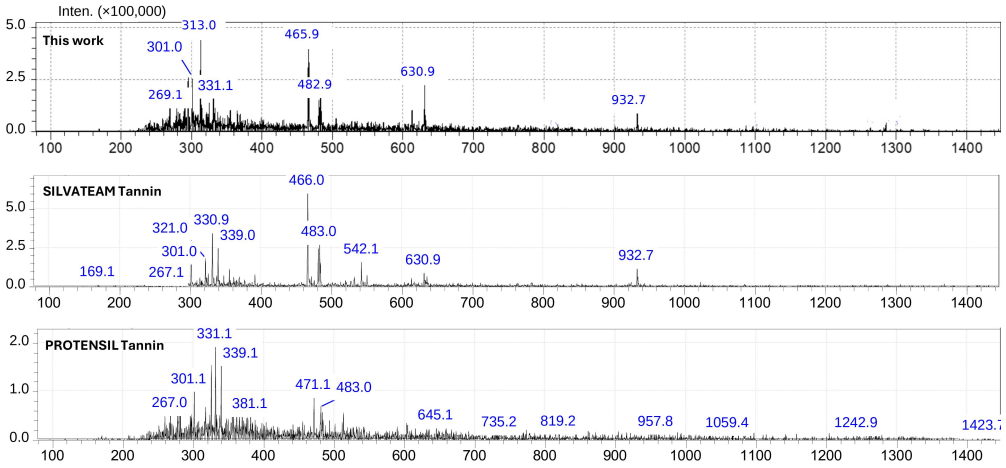


Figure 12. Negative-ion on-flow ESI mass spectra of the process-derived powder obtained in this work and the SILVATEAM and PROTENSIL commercial chestnut extracts.

3.6. Preserving a Second Value Chain for the Extracted Solid

The residual solid was evaluated by calorimetry and pelletization to distinguish preservation of specific energy content from preservation of pellet mechanical quality.

For LC, neither GCV nor NCV decreased appreciably after one or two pilot extraction cycles (Table 9); NCV remained within 18.1–18.2 MJ kg^{-1} dry basis.

Because extraction removes dry matter, unchanged NCV per kilogram should not be interpreted as conservation of the total initial energy inventory.

Pelletization provided a more demanding test of the residual solid. The extracted biomass could be densified using the same industrial procedure as the non-extracted material, but mechanical durability decreased from 97.5 to 90.9% and fines increased (Table 9). The extracted pellets were also visually darker.

Table 9. Energetic properties of LC before and after one and two extraction cycles and pellet-quality indicators for non-extracted and extracted residual chestnut biomass. Pelletization used the same industrial procedure in both cases.

Property	Non-Extracted	After Cycle 1	After Cycle 2/Extracted
GCV (MJ kg^{-1} dry basis)	19.5 ± 0.1	19.5 ± 0.1	19.6 ± 0.1
NCV (MJ kg^{-1} dry basis)	18.1 ± 0.1	18.1 ± 0.1	18.2 ± 0.1
Mechanical durability (%)	97.5	–	90.9
Fines (%)	0.9	–	3.8

The decrease in durability and increase in fines show that preservation of calorific value does not imply preservation of pellet quality. Removal of water-soluble extractives may alter surface chemistry or interparticle bonding, but the present data do not identify the mechanism. The extracted solid therefore remains a viable energy feedstock, although densification conditions would need re-optimization rather than direct transfer of the original pelletization procedure [2].

3.7. Integrated Process Implications

Table 10 summarizes extraction recovery, RO feed and final concentrations, and estimated dry-solids quantities on the stated reference bases.

Table 10. Stagewise material summary: extraction recovery, RO concentration, and dry-powder collection on the stated reference bases.

Process Stage	Feed/Calculation Basis	Main Outputs
Aqueous extraction—two successive contacts	1000 kg dry LR; two fresh-water contacts of 10,000 L each.	Liquid extracts: 139.1 kg dry solids. Extraction remainder: 860.9 kg dry matter, calculated by difference. [a]
High-concentration RO	Enriched feed: 78.90 g L^{-1} TSC. Dry-solids calculation basis: 1000 L of final concentrate.	Final concentrate: 283.73 g L^{-1} TSC. Estimated dry-solids content: 283.7 kg per 1000 L concentrate. [b]
Spray drying	1000 kg liquid feed at 20 wt.% TSC, containing 200 kg dry solids.	Collected powder: 120–124 kg dry solids, applying 60–62% collection recovery.

TSC: total solids concentration. Stage-specific reference bases are stated in the second column. [a] The extraction remainder includes residual biomass and solids in unrecovered liquid. [b] RO dry solids were estimated from the measured final TSC on the stated concentrate-volume basis.

The comparison in Table 11 shows that the individual operations perform within, and in several cases at the upper end of, representative literature ranges. The principal distinction of the present work, however, is process-level rather than a claim that every unit operation is universally superior. To the best of our knowledge, the complete experimental sequence—two residual chestnut biomass streams, aqueous extraction and extractant reuse, membrane selection and RO preconcentration, carrier-free spray drying, product benchmarking, and subsequent evaluation of calorific value and pelletization of the extracted solid—has not previously been reported within a single chestnut-biomass study.

The data identify three central interfaces. First, extraction yield must be balanced against water use: late fresh-water stages added little TPC, whereas reuse of the liquid phase increased solute loading and retained substantial extraction capacity. Second, RO and spray drying define a common concentration window. RO productivity deteriorated as the retentate became concentrated, while dryer recovery improved up to approximately 20% TSC but deteriorated at 30% TSC. The RO endpoint should therefore be selected from downstream sprayability rather than maximum membrane concentration. Third, extraction changes the allocation of value between soluble and solid fractions: the residual

biomass retained its specific calorific value but showed poorer pellet durability, so the second valorization route remains viable but requires its own process optimization.

Table 11. Positioning of the main process results against representative literature values. Comparisons are intended as benchmarking rather than strict ranking because feedstocks, analytical methods, equipment, and process objectives differ among studies.

Stage	This Work	Representative Literature and Positioning
Chestnut extraction	Up to 141 ± 7 mg GAE g^{-1} dry biomass; 90–93% of seven-stage TPC recovered within four stages	Aimone et al. reported 135.60 mg GAE g^{-1} dry matrix at laboratory scale and 95.96 mg GAE g^{-1} at semi-industrial scale [10]. The present maximum lies at the upper end of reported chestnut-wood values and is slightly higher numerically, without implying strict superiority.
RO retention	>99.9% apparent TPC retention; 96.5–97.6% TSC retention	Tapia-Quirós et al. reported >99.9% TPC rejection by RO [14], and Alsobh et al. reported >99% TPC retention by RO [25]. The present result is therefore at the upper end of reported global phenolic retention.
RO concentration	About 90% volume reduction in standard batches; limiting experiment approached 164 g GAE L^{-1} TPC and 284 g L^{-1} TSC	Conidi et al. reported 30.16 g L^{-1} total polyphenols after NF of chestnut-shell extract [15]; Lai et al. reported 25.82 g GAE L^{-1} polyphenols and 64.62 g L^{-1} total solids after RO of tea extract [27]. The present absolute concentrations are high, although matrix and method differences prevent direct ranking.
Spray drying	Maximum dry-solids recovery about 60–62%, carrier-free; powder TPC 450–497 mg GAE g^{-1}	Langrish and Premarajah reported 65–70% peak recovery [28]; Gavarić et al. reported 58.36% without carrier and 77.07% with 10% maltodextrin [29]. The present carrier-free recovery is competitive, and the single-cyclone laboratory configuration can under-recover fines relative to more complete collection trains [30].

The work establishes technical compatibility among the main operations across complementary laboratory and pilot campaigns. Together, the experiments define the principal process interfaces and provide a coherent basis for scale-up and integration. Further development can therefore focus on extending membrane operating time, evaluating direct RO-permeate reuse, accounting for feedstock variability, and refining post-extraction pelletization conditions.

4. Conclusions

This study shows that residual chestnut biomass can generate two experimentally relevant output streams: a water-soluble fraction that can be concentrated by RO and converted into a dry powder, and an extracted lignocellulosic solid that retains high specific calorific value. Four extraction stages recovered approximately 90–93% of the seven-stage Folin-reactive TPC response. RO provided near-complete apparent retention of the Folin-reactive response and major water removal, while carrier-free laboratory spray drying reached a maximum dry-solids collection recovery of approximately 60–62% in the favorable feed-solids region investigated. The resulting powder showed $a_w = 0.5850$, $d_{50} = 7.42$ µm, and a heterogeneous spray-dried morphology comprising spherical/subspherical and partially collapsed particles. Complementary FTIR, MALDI-TOF, SEC-GPC, and on-flow ESI-MS provided mutually supportive qualitative/size-distribution fingerprints. The extracted solid retained an NCV of approximately 18.1–18.2 MJ kg^{-1} dry basis, although pellet durability decreased.

Taken together, these findings support the technical feasibility of a cascading valorization strategy in which residual chestnut biomass yields both a phenolic-rich powder and an energy-relevant extracted solid. The combined extraction, extractant-reuse, RO, and spray-drying results define a practical operating window for liquid-stream valorization, while the retained NCV of the extracted solid supports its continued use in bioenergy applications. The study therefore provides a coherent experimental basis for further scale-up and process integration.

Supplementary Materials: Supporting information can be downloaded at: https://www.mdpi.com/article/10.3390/biomass6050090/s1, The supplementary file contains Table S1 (complete spray-drying dataset), Figure S1 (representative SEM micrographs), Figure S2 (differential and cumulative SEC-GPC molecular-size distributions), Figures S3 and S4 (individual FTIR spectra and fingerprint-region overlay), and Figures S5–S7 (MALDI-TOF spectra of the process-derived, PROTENSIL, and SILVATEAM extracts).

Author Contributions: Conceptualization, M.A.G.-A., J.R.Á.S. and S.L.; methodology, C.G.-R., L.G.-F., J.R.Á.S., M.A.G.-A., P.F.S. and S.L.; software, J.R.Á.S. and P.F.S.; validation, M.A.G.-A., P.F.S., J.R.Á.S. and S.L.; formal analysis, M.A.G.-A., J.R.Á.S., C.G.-R., L.G.-F., P.F.S. and S.L.; investigation, P.F.S.; resources, M.A.G.-A., J.R.Á.S., C.G.-R., L.G.-F. and P.F.S.; data curation, P.F.S., M.A.G.-A. and J.R.Á.S.; writing—original draft preparation, P.F.S. and C.G.-R.; writing—review and editing, M.A.G.-A., J.R.Á.S. and S.L.; visualization, C.G.-R., L.G.-F. and M.A.G.-A.; supervision, M.A.G.-A. and J.R.Á.S.; project administration, M.A.G.-A. and C.G.-R.; funding acquisition, M.A.G.-A., J.R.Á.S. and L.G.-F. All authors have read and agreed to the published version of the manuscript.

Funding: This work was supported by the Government of the Principality of Asturias (Spain) through the Institute of Economic Development of the Principality of Asturias (IDEPA), under project number IDE/2020/000473; by the Science, Technology and Innovation Plan (PCTI); and by the European Union through FEDER funding. PhD student Pablo Fernández Santos received a Severo Ochoa fellowship from the Government of the Principality of Asturias (grant number BP/20/135).

Institutional Review Board Statement: Not applicable.

Informed Consent Statement: Not applicable.

Data Availability Statement: The data supporting the findings of this study are available from the authors upon reasonable request.

Acknowledgments: The authors gratefully acknowledge the collaboration of Grupo Siero S.A. (Los Cuetos, Siero, Asturias, Spain) in the present study on the valorization of forest and sawmill residues. Their support, through the provision of the required biomass, was essential to the successful completion of this research. The authors also sincerely thank LERMaB (Laboratory for Studies and Research on Wood Material, University of Lorraine, France) for hosting Pablo Fernández Santos during a short research stay. During the preparation of this manuscript, the authors used ChatGPT (OpenAI; GPT-5.6 Sol) for language editing and the refinement of graphical elements. The authors reviewed and edited all outputs and take full responsibility for the content of this publication.

Conflicts of Interest: The authors declare no conflicts of interest. The funders had no role in the design of the study; in the collection, analyses, or interpretation of data; in the writing of the manuscript; or in the decision to publish the results.

Abbreviations

ATR-FTIR	Attenuated total reflectance Fourier-transform infrared spectroscopy
DMSO	Dimethyl sulfoxide
DPPH	2,2-Diphenyl-1-picrylhydrazyl
ESI-MS	Electrospray ionization mass spectrometry
FTIR	Fourier-transform infrared spectroscopy
GAE	Gallic acid equivalents
GCV	Gross calorific value
HPLC	High-performance liquid chromatography
IC_{50}	Half-maximal inhibitory concentration
LC	Residual biomass from old chestnut trees (local *caborno* source)
LR	Forestry and sawmilling chestnut residues
MALDI-TOF	Matrix-assisted laser desorption/ionization time-of-flight
MAPD	Mean absolute percentage deviation
MWCO	Molecular weight cut-off

NCV	Net calorific value
NF	Nanofiltration
PA-TFC	Polyamide thin-film composite
PEG	Polyethylene glycol
PES	Polyethersulfone
PP	Polypropylene
PS	Polysulfone
PVDF	Polyvinylidene fluoride
RO	Reverse osmosis
S/L	Solid-to-liquid ratio
SEC-GPC	Size-exclusion chromatography–gel permeation chromatography
SEM	Scanning electron microscopy
TCH	Total carbohydrate content
TMP	Transmembrane pressure
TPC	Total phenolic content
TSC	Total solids content
UF	Ultrafiltration
VRF	Volume reduction factor

References

1. Contreras, M.d.M.; Lama-Muñoz, A.; Gutiérrez-Pérez, J.M.; Espínola, F.; Moya, M.; Romero, I.; Castro, E. Integrated Process for Sequential Extraction of Bioactive Phenolic Compounds and Proteins from Mill and Field Olive Leaves and Effects on the Lignocellulosic Profile. *Foods* **2019**, *8*, 531. [CrossRef] [PubMed]
2. Jusic, J.; Filieri, A.; Crognale, S.; Manni, M.; Tamantini, S.; Vinciguerra, V.; Cardarelli, A.; Barbanera, M.; Jones, D.; Matt, D.; et al. Chestnut Wood Residues, with and Without Tannins, as a Potential Feedstock for PHA Bioplastic Production. *Polymers* **2026**, *18*, 1206. [CrossRef] [PubMed]
3. Pizzi, A. Chapter 8 - Tannins: Major Sources, Properties and Applications. In *Monomers, Polymers and Composites from Renewable Resources*; Belgacem, M.N., Gandini, A., Eds.; Elsevier: Amsterdam, The Netherlands, 2008; pp. 179–199. [CrossRef]
4. Ciriminna, R.; Meneguzzo, F.; Li Petri, G.; Meneguzzo, C.; Angellotti, G.; Pagliaro, M. Chestnut Tannin: New Use, Research and Bioeconomy. *J. Bioresour. Bioprod.* **2024**, *9*, 246–252. [CrossRef]
5. Comandini, P.; Lerma-García, M.J.; Simó-Alfonso, E.F.; Toschi, T.G. Tannin Analysis of Chestnut Bark Samples (*Castanea sativa* Mill.) by HPLC-DAD-MS. *Food Chem.* **2014**, *157*, 290–295. [CrossRef] [PubMed]
6. Khatib, M.; Campo, M.; Bellumori, M.; Cecchi, L.; Vignolini, P.; Innocenti, M.; Mulinacci, N. Tannins from Different Parts of the Chestnut Trunk (*Castanea sativa* Mill.): A Green and Effective Extraction Method and Their Profiling by HPLC-DAD-MS. *ACS Food Sci. Technol.* **2023**, *3*, 1903–1912. [CrossRef]
7. Raposo, F.; Borja, R.; Gutiérrez-González, J.A. A Comprehensive and Critical Review of the Unstandardized Folin-Ciocalteu Assay to Determine the Total Content of Polyphenols: The Conundrum of the Experimental Factors and Method Validation. *Talanta* **2024**, *272*, 125771. [CrossRef] [PubMed]
8. Gironi, F.; Piemonte, V. Temperature and solvent effects on polyphenol extraction process from chestnut tree wood. *Chem. Eng. Res. Des.* **2011**, *89*, 857–862. [CrossRef]
9. Capparucci, C.; Gironi, F.; Piemonte, V. Equilibrium and extraction kinetics of tannins from chestnut tree wood in water solutions. *Asia-Pacific J. Chem. Eng.* **2011**, *6*, 606–612. [CrossRef]
10. Aimone, C.; Grillo, G.; Boffa, L.; Giovando, S.; Cravotto, G. Tannin Extraction from Chestnut Wood Waste: From Lab Scale to Semi-Industrial Plant. *Appl. Sci.* **2023**, *13*, 2494. [CrossRef]
11. Karaseva, V.; Bergeret, A.; Lacoste, C.; Ferry, L.; Fulcrand, H. Influence of Extraction Conditions on Chemical Composition and Thermal Properties of Chestnut Wood Extracts as Tannin Feedstock. *ACS Sustain. Chem. Eng.* **2019**, *7*, 17047–17054. [CrossRef]
12. Bucić-Kojić, A.; Planinić, M.; Tomas, S.; Bilić, M.; Velić, D. Study of solid–liquid extraction kinetics of total polyphenols from grape seeds. *J. Food Eng.* **2007**, *81*, 236–242. [CrossRef]
13. Das, I.; Arora, A. Kinetics and mechanistic models of solid-liquid extraction of pectin using advance green techniques—A review. *Food Hydrocoll.* **2021**, *120*, 106931. [CrossRef]
14. Tapia-Quirós, P.; Montenegro-Landívar, M.F.; Reig, M.; Vecino, X.; Saurina, J.; Granados, M.; Cortina, J.L. Integration of Nanofiltration and Reverse Osmosis Technologies in Polyphenols Recovery Schemes from Winery and Olive Mill Wastes by Aqueous-Based Processing. *Membranes* **2022**, *12*, 339. [CrossRef] [PubMed]

15. Conidi, C.; Donato, L.; Algieri, C.; Cassano, A. Valorization of Chestnut Processing By-Products: A Membrane-Assisted Green Strategy for Purifying Valuable Compounds from Shells. *J. Clean. Prod.* **2022**, *378*, 134564. [CrossRef]
16. Assadpour, E.; Jafari, S.M. Advances in Spray-Drying Encapsulation of Food Bioactive Ingredients: From Microcapsules to Nanocapsules. *Annu. Rev. Food Sci. Technol.* **2019**, *10*, 103–131. [CrossRef] [PubMed]
17. Baccarin, T.; Debrassi, A.; de Souza, M.M.; Yunes, R.A.; Malheiros, Â.; Silva, R.M.L. Influence of Process Conditions on Physicochemical Properties and Antinociceptive Activity in Vivo of Spray-Dried Rapanea ferruginea Mez. Stem Bark Extract. *Powder Technol.* **2016**, *291*, 66–74. [CrossRef]
18. Singleton, V.L.; Rossi, J.A. Colorimetry of Total Phenolics with Phosphomolybdic-Phosphotungstic Acid Reagents. *Am. J. Enol. Vitic.* **1965**, *16*, 144–158. [CrossRef]
19. *ISO 18787:2017*; Foodstuffs—Determination of Water Activity. International Organization for Standardization: Geneva, Switzerland, 2017.
20. Kakavas, K.V.; Chavenetidou, M.; Birbilis, D. Chemical Properties of Greek Stump Chestnut (*Castanea sativa* Mill.). *Nat. Prod. Chem. Res.* **2018**, *6*, 331. [CrossRef]
21. Chiarini, A.; Micucci, M.; Malaguti, M.; Budriesi, R.; Ioan, P.; Lenzi, M.; Fimognari, C.; Gallina Toschi, T.; Comandini, P.; Hrelia, S. Sweet Chestnut (*Castanea sativa* Mill.) Bark Extract: Cardiovascular Activity and Myocyte Protection against Oxidative Damage. *Oxidative Med. Cell. Longev.* **2013**, *2013*, 471790. [CrossRef] [PubMed]
22. Pinto, P.C.R.; Mota, I.F.; Loureiro, J.M.; Rodrigues, A.E. Membrane Performance and Application of Ultrafiltration and Nanofiltration to Ethanol/Water Extract of Eucalyptus Bark. *Sep. Purif. Technol.* **2014**, *132*, 234–243. [CrossRef]
23. Pinto, P.R.; Mota, I.F.; Pereira, C.M.; Ribeiro, A.M.; Loureiro, J.M.; Rodrigues, A.E. Separation and Recovery of Polyphenols and Carbohydrates from Eucalyptus Bark Extract by Ultrafiltration/Diafiltration and Adsorption Processes. *Sep. Purif. Technol.* **2017**, *183*, 96–105. [CrossRef]
24. Cifuentes-Cabezas, M.; Carbonell-Alcaina, C.; Vincent-Vela, M.C.; Mendoza-Roca, J.A.; Álvarez-Blanco, S. Comparison of Different Ultrafiltration Membranes as First Step for the Recovery of Phenolic Compounds from Olive-Oil Washing Wastewater. *Process Saf. Environ. Prot.* **2021**, *149*, 724–734. [CrossRef]
25. Alsobh, A.; Zin, M.M.; Vatai, G. Comparison of reverse osmosis (X-20, RO-99) and nanofiltration (NF-270) membranes in the concentration of hawthorn fruit and anise seed extracts. *Int. J. Food Sci. Technol.* **2024**, *59*, 3087–3096. [CrossRef]
26. Romero-Dondiz, E.M.; Almazán, J.E.; Rajal, V.B.; Castro-Vidaurre, E.F. Comparison of the Performance of Ultrafiltration and Nanofiltration Membranes for Recovery and Recycle of Tannins in the Leather Industry. *J. Clean. Prod.* **2016**, *135*, 71–79. [CrossRef]
27. Lai, Q.D.; Doan, N.T.T.; Nguyen, H.D. Technical assessment of reverse osmosis for concentration of fresh tea leaf extract. *J. Food Process Eng.* **2021**, *44*, e13725. Correction in *J. Food Process Eng.* **2021**, *44*, e13830. [CrossRef]
28. Langrish, T.A.G.; Premarajah, R. Antioxidant capacity of spray-dried plant extracts: Experiments and simulations. *Adv. Powder Technol.* **2013**, *24*, 771–779. [CrossRef]
29. Gavarić, A.; Vladić, J.; Ambrus, R.; Jokić, S.; Szabó-Révész, P.; Tomić, M.; Blažić, M.; Vidović, S. Spray Drying of a Subcritical Extract Using Marrubium vulgare as a Method of Choice for Obtaining High Quality Powder. *Pharmaceutics* **2019**, *11*, 523. [CrossRef] [PubMed]
30. Sosnik, A.; Seremeta, K.P. Advantages and challenges of the spray-drying technology for the production of pure drug particles and drug-loaded polymeric carriers. *Adv. Colloid Interface Sci.* **2015**, *223*, 40–54. [CrossRef] [PubMed]

Disclaimer/Publisher's Note: The statements, opinions and data contained in all publications are solely those of the individual author(s) and contributor(s) and not of MDPI and/or the editor(s). MDPI and/or the editor(s) disclaim responsibility for any injury to people or property resulting from any ideas, methods, instructions or products referred to in the content.